MOLECULAR AND CELLULAR BIOLOGY, Dec. 2009, p. 6294–6308 Vol. 29, No. 23
0270-7306/09/$12.00 doi:10.1128/MCB.00939-09

Hepatocyte Nuclear Factor 4α, a Key Factor for Homeostasis, Cell Architecture, and Barrier Function of the Adult Intestinal Epithelium▽

Anne-Laure Cattin,[1,2,3] Johanne Le Beyec,[1,2,3] Frederick Barreau,[4] Susan Saint-Just,[1,2,3,5] Anne Houllier,[1,2,3] Frank J. Gonzalez,[6] Sylvie Robine,[7] Martine Pinçon-Raymond,[1,2,3] Philippe Cardot,[1,2,3] Michel Lacasa,[1,2,3] and Agnès Ribeiro[1,2,3]*

Centre de Recherche des Cordeliers, Université Pierre et Marie Curie—Paris 6, UMRS 872, Paris F-75006, France[1]; INSERM, U872, Paris F-75006, France[2]; Université Paris Descartes, UMRS 872, Paris F-75006, France[3]; Laboratoire de Pharmacologie Cellulaire et Moléculaire, Ecole Pratique des Hautes Etudes, Paris F-75006, France[4]; Morphogenesis and Intracellular Signaling, UMR 144, Institut Curie-CNRS, Paris, France[5]; Laboratory of Metabolism, Center for Cancer Research, National Cancer Institute, National Institutes of Health, Bethesda, Maryland[6]; and UMR-S843 INSERM, Université Paris Diderot, Service de Gastroentérologie, Hôpital R. Debré, AP-HP, Paris, France[7]

Received 17 July 2009/Returned for modification 20 August 2009/Accepted 17 September 2009

Hepatocyte nuclear factor 4α (HNF-4α) is a transcription factor which is highly expressed in the intestinal epithelium from duodenum to colon and from crypt to villus. The homeostasis of this constantly renewing epithelium relies on an integrated control of proliferation, differentiation, and apoptosis, as well as on the functional architecture of the epithelial cells. In order to determine the consequences of HNF-4α loss in the adult intestinal epithelium, we used a tamoxifen-inducible Cre-loxP system to inactivate the *Hnf-4a* gene. In the intestines of adult mice, loss of HNF-4α led to an increased proliferation in crypts and to an increased expression of several genes controlled by the Wnt/β-catenin system. This control of the Wnt/β-catenin signaling pathway by HNF-4α was confirmed in vitro. Cell lineage was affected, as indicated by an increased number of goblet cells and an impairment of enterocyte and enteroendocrine cell maturation. In the absence of HNF-4α, cell-cell junctions were destabilized and paracellular intestinal permeability increased. Our results showed that HNF-4α modulates Wnt/β-catenin signaling and controls intestinal epithelium homeostasis, cell function, and cell architecture. This study indicates that HNF-4α regulates the intestinal balance between proliferation and differentiation, and we hypothesize that it might act as a tumor suppressor.

Hepatocyte nuclear factor 4 (HNF-4) belongs to the superfamily of nuclear receptors (8). In mammals, it is represented by two paralogs: HNF-4α, which is expressed in the liver, kidneys, pancreas, and intestine, and HNF-4γ, which is expressed in the same organs except the liver (14, 42, 50). HNF-4γ has not been extensively studied. However, mice lacking expression of the *Hnf-4g* gene do not present an overt phenotype (19). HNF-4α has been essentially studied in liver and hepatocyte cell lines. Mutations in the human *Hnf-4a* gene are associated with maturity onset diabetes of the young (MODY1), a disorder that is characterized by the early onset of type 2 diabetes (20). Disruption of *Hnf-4a* gene expression leads to embryonic death at the gastrulation stage (embryonic day 6.5) (15). HNF-4α is dispensable for hepatic specification but necessary for hepatoblast differentiation into hepatocytes (29). Inactivation of the *Hnf-4a* gene in fetal liver revealed that HNF-4α also controls epithelial morphology (41), and transcriptome analysis of *Hnf-4a* knockout in fetal liver showed that genes encoding proteins of all categories of cell junctions (adherens, desmosomes, tight) are targets of HNF-4α (5). Expression of HNF-4α in dedifferentiated hepatocytes provokes the reexpression of epithelial markers, such as E-cadherin (48). Its ectopic expression in mesenchymal cells induces the expression and the proper localization of tight and adherens junction proteins (10, 41), as well as the formation of microvilli (12), suggesting that HNF-4α is a central regulator of epithelial morphogenesis. In adult mouse liver, conditional disruption of the *Hnf-4a* gene revealed a key role for HNF-4α in the control of genes involved in amino acid, glucose, and lipid metabolism (21). All together, these studies show that HNF-4α is at the crossroads between liver morphogenesis and function (43). By contrast, the role of HNF-4α in the intestine is less well understood.

The intestinal epithelium establishes a physical barrier between the external and internal compartments and plays a key role in the absorption and transfer of nutrients. These functions, in constantly renewing tissue, rely on the functional architecture of the epithelial cells, as well as on the complex and precise control of proliferation, differentiation, and apoptosis to ensure the homeostasis of the intestinal epithelium (46). The permanent renewal of epithelial cells is accomplished by the stem cells located at the bottom of the crypts that generate four differentiated cell types in strictly controlled proportions: Paneth cells, goblet cells, enteroendocrine cells, and the absorptive enterocytes which represent 90% of the intestinal epithelial cells. The last three cell types differentiate during their migration upward from crypts toward the tips of the villi, where they die by apoptosis and are shed into the lumen (17, 33), the entire process being completed within 3 to 5 days in mice for

* Corresponding author. Mailing address: UMRS 872, 15 rue de l'école de médecine, 75006 Paris, France. Phone: 33 1 42 34 69 18. Fax: 33 1 43 25 16 15. E-mail: agnes.ribeiro-pillet@crc.jussieu.fr.

▽ Published ahead of print on 5 October 2009.

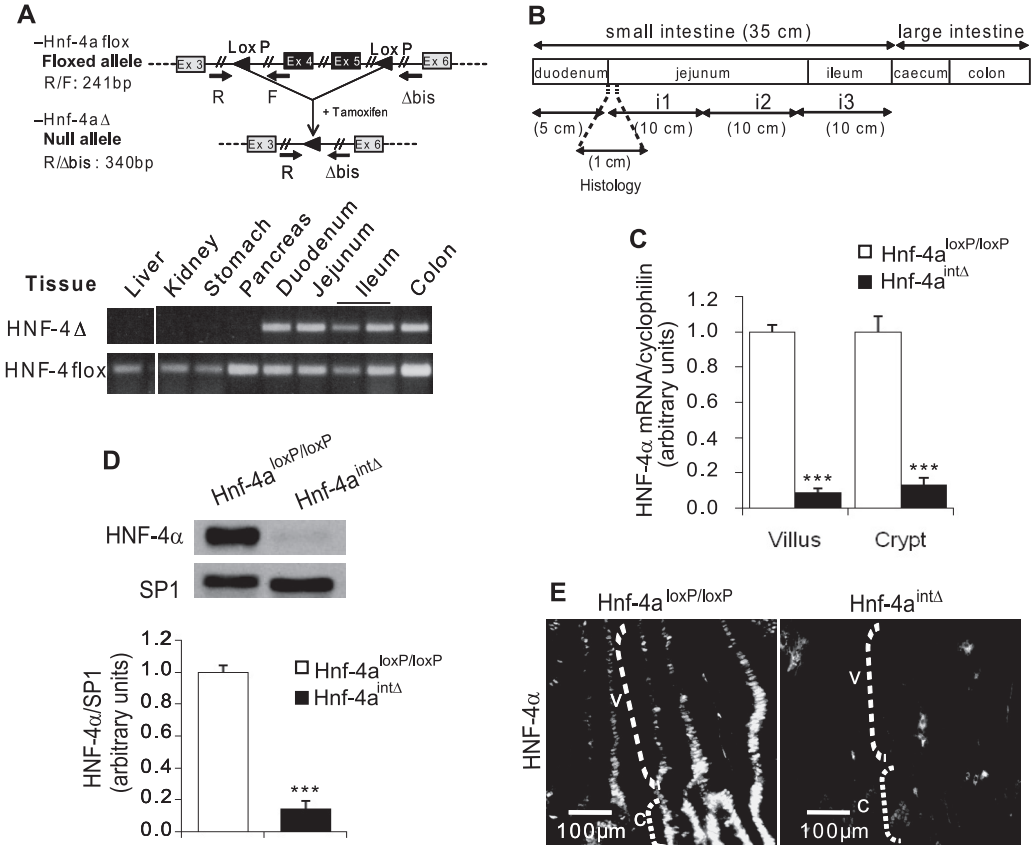

FIG. 1. Induction of CreERT2 recombinase leads to specific loss of HNF-4α in the epithelium of the adult mouse small intestine. (A) Schematic representation of the gene with the positions of the three primers used for genotyping (top) and identification of the recombination of the *Hnf-4a* gene by PCR analysis of genomic DNA from various tissues (bottom). The 340-bp fragment and the 241-bp fragment originate, respectively, from the recombined and intact alleles. The epithelium was obtained by scraping, and the contaminating mesenchyme, where the villin promoter is not active, is at the origin of the 241-bp fragment in the five intestinal samples. Recombination is only detectable in the intestine. (B) Schematic representation of the intestinal cephalocaudal axis. The i1 part of the jejunum was taken to perform RNA and protein analyses. About 1 cm of the proximal jejunum was removed for histological analyses. (C) Quantification of *Hnf-4a* mRNA levels in epithelial cells from villi and crypts of the jejunum by quantitative RT-PCR. mRNA levels are expressed relative to the amount present in *Hnf-4a*$^{loxP/loxP}$ mice and were normalized to that of cyclophilin. (D) Representative Western blot analysis and quantification of HNF-4α protein in epithelial cells from the jejunums of control *Hnf-4a*$^{loxP/loxP}$ and *Hnf-4a*$^{int\Delta}$ mice. The level of HNF-4α is expressed relative to the amount present in *Hnf-4a*$^{loxP/loxP}$ mice and is normalized to that of SP1. (E) Immunofluorescent staining of HNF-4α in the jejunums of *Hnf-4a*$^{loxP/loxP}$ and *Hnf-4a*$^{int\Delta}$ mice. Crypts and villi are indicated by the letters C and V, respectively. For each graph, an unpaired Student *t* test was used to measure significance. ***, $P < 0.001$. Error bars indicate the standard error of the mean.

enterocytes. The fourth cell type, i.e., Paneth cells, is located in the bottom of the crypts. The precise molecular mechanisms sustaining these proliferation/differentiation/apoptosis events are not well understood. Besides cell-cell contacts and epithelium-mesenchyme interactions, different transcription factors have been implicated in these events, among which are Cdx1, Cdx2, and GATA4, -5, and -6. Results from our group (2, 9, 45) and from studies based on transcriptome, metabolome, and bioinformatic analyses have suggested an important role for HNF-4α in the regulation of the enterocyte phenotype (30, 35, 49). Recently, it has been shown that HNF-4α is essential for the normal embryonic development of the mouse colon (18).

The aim of the present study was to determine the role of HNF-4α in the adult mouse small intestine. Using an inducible and tissue-specific Cre-loxP system to circumvent the early embryonic lethality of HNF-4α knockout mice, we generated adult mice lacking HNF-4α in the intestinal epithelium and demonstrated that HNF-4α plays a pivotal role in the homeostasis of the intestinal epithelium, in the epithelial cell architecture, and in the barrier function of the intestine.

MATERIALS AND METHODS

Generation of HNF-4α mutant mice. *Hnf-4a*$^{loxP/loxP}$ mice harboring an *Hnf-4a* allele in which exons 4 and 5 were flanked by *loxP* sites (Fig. 1A) have been described previously (21). The tamoxifen-dependent 9-kb-villin-Cre-ERT2 recombinase mouse transgenic line (16) was used to produce inducible and intestinal epithelium-specific inactivation of the *Hnf-4a* gene. villin-Cre-ERT2 mice were mated with *Hnf-4a*$^{loxP/+}$ mice to obtain *Hnf-4a*$^{loxP/loxP}$; villin-Cre-ERT2 mice. Mice were genotyped by PCR of tail biopsy DNA with previously described primers (16, 21). The Cre recombinase activation in intestinal epithelial cells was induced by daily intraperitoneal injection of 600 μg/15 μl (ethanol/phosphate-buffered saline [PBS], vol/vol) tamoxifen (Sigma) for 5 days as previously described (53). Mice were euthanized on day 8 following the first injection. Two strains were utilized in this study, *Hnf-4a*$^{loxP/loxP}$ as control mice and *Hnf-4a*$^{loxP/loxP}$; villin-Cre-ERT2 as *Hnf-4a*$^{int\Delta}$ mice (where *int* stands for intestinal and Δ stands

for deletion), both receiving tamoxifen treatment. The recombined allele was detected with the R primer described in reference 21 and the Δbis primer 5′-TGCTCCGTAGGAAGTCACAGG-3′ (Fig. 1A) after rough scraping of the intestine to prepare the epithelial sample for genotyping. Experimental mice were 2-month-old males fed a standard diet ad libitum. The animal care and experimental procedures used in this study conform to the French guidelines for animal studies.

Tissue isolation and histology. Mice were euthanized, and their intestines were removed and flushed gently with PBS. The small intestine was taken out after the duodenum and cut into three equal parts named i1, i2, and i3 (Fig. 1B). For histological analyses, pieces of the proximal jejunum (1 cm) (Fig. 1B) were immediately embedded in tissue-tek or fixed overnight at 4°C in alcohol-formalin-acetic acid before being embedded in paraffin. Immunostaining with anti-chromogranine A, anti-bromodeoxyuridine (anti-BrdU), and anti-caspase 3 antibodies was performed with 5-μm paraffin sections. Histological colorations and other immunostainings were performed with 6-μm cryosections. Periodic acid-Schiff (PAS) (32) staining was performed by using a standard histological protocol (28). Immunostaining was performed as previously described (38). The primary antibodies used were goat anti-HNF-4α (1/250), goat anti-HNF-4γ (1/5,000) (C-19 and C-18, respectively; Santa Cruz Biotechnology), rabbit anti-lysozyme (1/200) (A0099; Dako), rabbit anti-active caspase 3 (1/100) (557035; BD Pharmingen), rabbit anti-chromogranin A (1/200), rabbit anti-Ki67 (1/100) (ab45138 and ab15580, respectively; Abcam), rat anti-BrdU (1/50) (ab6326; Abcam), rabbit anti-EBP50 (1/100) (PA1-090; Affinity Bioreagents), and mouse anti-E-cadherin (1/250) (ECCD-2; Zymed Laboratories). The secondary antibodies were Alexafluor-conjugated donkey anti-goat 546, goat anti-rat 488, and donkey anti-rabbit 488 (Molecular Probes). Nuclear counterstaining was performed with 4′,6-diamidino-2-phenylindole (DAPI). Immunostaining was examined by epifluorescence microscopy (Axiophot microscope connected to an Axiocam camera using the Axiovision 4.5 software; Carl Zeiss). The β-catenin staining was performed according to standard procedures described previously (44), with mouse anti-β-catenin at 1/50 (610154; Transduction Laboratories). A horseradish peroxidase-labeled secondary antibody (Amersham Biosciences) and 3,3′-diaminobenzidine were employed for revelation.

Electron microscopy. Fragments of the proximal jejunum (1 cm) were prepared as previously described (38). Observations were made with a JEOL CX100 electron microscope equipped with a Gatan digital camera (3.11.0), and the micrographs were processed with Gatan software.

Cell proliferation. Eight days after the first tamoxifen injection, mice were injected intraperitoneally with 120 mg BrdU (Sigma) per kg of body weight and sacrificed 90 min later. Paraffin sections of alcohol-formalin-acetic acid-fixed jejunum were incubated for 30 min in 2.5 N HCl before processing for immunostaining with anti-BrdU antibody (Abcam). Antigen retrieval was performed by boiling slides in 10 mM citrate buffer (pH 6) for 10 min. After washes in PBS, immunostaining was done as described above, with a 1/50 dilution of a BrdU-directed monoclonal antibody.

Epithelial cell recovery. The epithelium from villi and crypts was isolated as previously described (2, 45), with Cell Recovery Solution (BD Biosciences) and a chelating buffer, respectively. The enrichment of epithelial cells of villi versus the epithelial cells of crypts, and reciprocally, was measured by the mRNA levels of *apoA4*, a gene specific for enterocytes and those of *Lgr5*, a gene specifically expressed in the stem cells of crypts. The ratio of the mRNA levels in the two compartments expresses the enrichment factor. The level of *apoA4* mRNA is 7-fold higher in the villus fraction than in the crypt fraction, and that of *Lgr5* mRNA is, reciprocally, 7.36-fold higher in the crypt fraction than in the villus fraction, indicating a 7-fold enrichment in each fraction. Normalization was done with cyclophilin mRNA.

RNA extraction and gene expression analysis. Total RNA from villus or crypt epithelial cells from the mouse jejunum (i1) was isolated by using RNAplus reagent (qBiogene) according to the manufacturer's instructions. Reverse transcription (RT) was performed with 1 μg of RNA in a 20-μl reaction mixture. Semiquantitative real-time PCR was performed with the LightCycler system by using SYBR green according to the manufacturer's procedures (Roche Molecular Biochemicals). The sequences of the primers used are reported in Table 1. After tamoxifen injection, the activated Cre recombinase deleted exons 4 and 5 of the *Hnf-4a* gene. The loss of normal HNF-4α mRNA was quantified with primers located in exons 3 and 5. Results are expressed as the ratio of the mRNA of interest to cyclophilin mRNA.

Protein extraction and Western blot analysis. Total proteins from the villus epithelial cells from mouse jejunum (i1) were isolated with a lysis buffer (20 mM Tris, 150 mM NaCl, 5 mM EDTA, 1% Triton X-100, 0.5% sodium deoxycholate) containing a protease inhibitor cocktail (Sigma). Nuclear and cytoplasmic proteins from villus or crypt epithelial cells of the jejunum were isolated with the NE-PER nuclear and cytoplasmic extraction reagent kit (Pierce). Protein concentrations were measured with the Bio-Rad DC protein assay (Bio-Rad). For sodium dodecyl sulfate (SDS)-polyacrylamide gel electrophoresis, samples with equal amounts of protein were boiled for 10 min in SDS-reducing buffer and separated on a 0.1% SDS-containing polyacrylamide gel. Proteins were transferred onto nitrocellulose membranes and probed with primary antibodies. The primary antibodies used were goat anti-HNF-4α (1/5,000), rabbit anti-p21 (1/1,000) (C-19 and H-164, respectively; Santa Cruz Biotechnology), rabbit anti-claudin 7 (1/2,000), rabbit anti-claudin 2 (1/2,000), rabbit anti-ZO-1 (1/100) (34-9100 32-5600 and 61-7300, respectively; Zymed Laboratories), rabbit anti-EBP50 (1/2,000) (PA1-090; Affinity Bioreagents), rat anti-E-cadherin (1/2500) (ECCD-2; Takara), mouse anti-β-catenin (1/2,000) (610154; BD Transduction Laboratories), mouse anti-actin (1/2,000) (MAB1501R; Chemincon), rabbit anti-LDH (lactate dehydrogenase) (1/20,000) (ab52488; Abcam), and rabbit anti-SP1 (1/1,000) (PEP-2; Santa Cruz Biotechnology). A horseradish peroxidase-labeled secondary antibody (Amersham Biosciences) was used and detected by the chemiluminescence method (ECL; Amersham Biosciences). The quantitative analyses were performed with a high-performance calibrated imaging densitometer (Bio-Rad GS-800) by using PD Quest and ImageQuant 5.2 software. Results are expressed as the ratio of the protein of interest to Sp1 for nuclear proteins or actin for cytoplasmic proteins.

Measurement of intestinal permeability. In vivo paracellular permeability was measured as previously described after mice were given an oral bolus of fluorescein isothiocyanate-labeled dextran 4 kDa (FITC-dextran; Sigma) of 60 mg/100 g body weight (40). The paracellular permeability of the ileal mucosa was assessed in 0.196-cm^2 Ussing chambers by measuring the mucosal-to-serosal flux of FITC-dextran as previously described (4). FITC-dextran was assayed by fluorimetry (excitation wavelength, 490 nm; emission wavelength, 520 nm). Mucosal-to-serosal flux was expressed as picomoles per hour per square centimeter of ileal mucosa.

Plasmids, transfection experiments, and Tcf/β-catenin reporter assay. The vectors encoding rat HNF-4α2 (pMT2-HNF-4α) and β-galactosidase (pRSV-β-Gal) were as previously described (2). The T-cell factor (TCF)-responsive TOPflash vector (Millipore) expressing luciferase driven by multiple TCF-responsive elements was utilized to evaluate the activity of β-catenin. TCF-responsive elements were mutated into the FOPflash vector (Millipore) used as a negative control. HCT116 human colorectal cancer cells were plated into 12-well plates at 10^5 per well and grown in Dulbecco modified Eagle medium supplemented with 10% fetal bovine serum (Invitrogen) maintained at 37°C in a humidified, 5% CO_2-containing atmosphere. Transfection was performed 72 h after plating by using Lipofectamine 2000 (Invitrogen) according to the manufacturer's instructions. Cells were transfected with 200 ng of TOP or FOP vector along with 300 ng RSV-βGal plasmid and increasing amounts of PMT2-HNF-4α. Cells were then harvested at 48 h posttransfection. β-Galactosidase and luciferase assays were performed with a luminometer and a microplate reader. Luciferase activity was normalized to β-galactosidase activity.

Coimmunoprecipitation. The plasmid encoding Flag-Tcf4 was a generous gift from M. Idogawa (23, 24). Caco-2/TC7 cells were cultured in Dulbecco modified Eagle medium supplemented with 20% heat-inactivated fetal bovine serum and antibiotics. HCT116 cells were cultivated and transfected with plasmid encoding HNF-4α and Flag-Tcf4 as described previously. Cells were lysed on ice in a mixture of 50 mM Tris HCl (pH 8.0), 150 mM NaCl, 5 mM EGTA (pH 8.0), 50 mM NaF (pH 8.0), 10% glycerol, 1.5 mM $MgCl_2$, and 1% Triton X-100 containing freshly added protease inhibitor cocktail (Sigma). Lysates were clarified by centrifugation at 4°C; protein concentrations were determined with a bicinchoninic acid protein quantification kit (Interchim). Immunoprecipitations were performed overnight at 4°C with rabbit, mouse, and goat control immunoglobulins G (IgG; Santa Cruz Biotechnology), mouse anti-β-catenin (610154; BD Transduction Laboratories), rabbit anti-HNF-4 (H-171; Santa Cruz Biotechnology), mouse anti-Flag (M2; Sigma), or rabbit anti-Tcf4 (H-125; Santa Cruz Biotechnology) antibodies. Five micrograms of each antibody or control IgG was used for 1 mg of transfected HCT116 and CaCo-2/TC7 cell extracts. Immunocomplexes were collected on protein A-Sepharose beads and protein G-Sepharose beads (GE Healthcare) during the last 45 min. The beads were pelleted by centrifugation, washed three times with a mixture of Tris HCl (pH 8.0), 150 mM NaCl, 5 mM EGTA, and 1% NP-40 and then boiled for 10 min in SDS sample buffer. Western blots were probed with goat anti-HNF-4α (1/5,000) (C-19; Santa Cruz Biotechnology), goat anti-Tcf4 (1/2,000) (N-20; Santa Cruz Biotechnology), and mouse anti-β-catenin (1/2,000).

Statistical tests. Results were expressed as means ± the standard errors of the means. The statistical significance of differences was determined by an unpaired Student *t* test by using Excel software.

TABLE 1. Sequences of the primers used for semiquantitative RT-PCR[a]

Primer	Sequence (5′→3′)	
	Forward	Reverse
Cyclophilin	TGGAGAGCACCAAGACAGACA	TGCCGGAGTCGACAATGAT
Apo B	GCCCATTGTGGACAAGTTGATC	CCAGGACTTGGAGGTCTTGGA
Apo A4	GACTACTTCAGCCAAAACAGTTGGA	AAGCTGCCTTTCAGGTTCTCCT
Axin2	GAGAGTGAGCGGCAGAGC	CGGCTGACTCGTTCTCCT
Cck	TGATTTCCCCATCCAAAGC	GCTTCTGCAGGGACTACCG
Cdh-1	TCCTTGTTCGGCTATGTGTC	GGCATGCACCTAAGAATCAG
Cdx 1	TCCGAGCTGGCTGCTAAC	CGGTTCTGGAACCAGATCTTT
Cdx 2	CACCATCAGGAGGAAAAGTGA	CTGCGGTTCTGAAACCAAAT
Claudin-2	GGCTGTTAGGCACATCCAT	TGGCACCAACATAGGAACTC
Claudin-3	AAGCCGAATGGACAAAGAA	CTGGCAAGTAGCTGCAGTG
Claudin-4	CGCTACTCTTGCCATTACG	ACTCAGCACACCATGACTTG
Claudin-7	AGGGTCTGCTCTGGTCCTT	GTACGCAGCTTTGCTTTCA
Claudin-12	GTCCTCTCCTTTCTGGCAAC	ATGTCGATTTCAATGGCAGA
Claudin-15	GCTTCTTCATGTCAGCCCTG	TTCTTGGAGAGATCCATGTTGC
Crypt 1	TCAAGAGGCTGCAAAGGAAGA	ACCCTTTCTGCAGGTTCCATT
Cyclin D1	AAGTTCATTTCCAACCCACCC	TGGAAAGAAAGTGCGTTGTGC
Dsk2	TGCAGTTCCCATTCGAGTTACAGACAGA	TTGATGCCCGGGAAACACTACAGACTAAT
EBP50	AGGTCAATGGTGTCTGCATG	TGCTGAAGGGCTCAGGCAAG
F11r	CGAGGGGAAAGCCGGGAGGAAACTGTTGTT	CCGCATAGGGAGCTGTGATCTGGCTGTTAT
FABP-I	TTACCAGAAACCTCTCGGACA	TTACCAGAAACCTCTCGGACA
Gcg	CACGCCCTTCAAGACACAG	GTCCTCATGCGCTTCTGTC
Gip	CAGGTAGGAGGAGAAGACCTCA	CCTAGATTGTGTCCCCTAGCC
Gjb 1*	GATGAGAAGTCCTCTTTCATCTGTAAC	GGTCATAGCAGACGCTGTTG
Hes 1	TCAACACGACACCGGACAAA	TTATTCTTGCCCTTCGCCTC
HNF-1alpha	AGAACCTCAGCCCAGAGGAG	TGTGCTGCTGCAAGTACGA
HNF-1beta	ATCCCCAGCAATCTCAGAAC	GCTTGGGAGGTGTTGAGG
HNF-4alpha	CAGTGTCGTTACTGCAGGC (exon3)	GATGGGAGAGGTGATCTGTTG (exon5)
HNF-4gamma	CTGCTGTTGCTGCTGCCA	CAGTGTGGACATGGGACC
Klf4	CGGGAAGGGAGAAGACACT	GAGTTCCTCACGCCAACG
Lgr5	CTTCACTCGGTGCAGTGCT	CAGCCAGCTACCAAATAGGTG
Math 1*	TGCGATCTCCGAGTGAGAG	CTCTTCTGCAAGGTCTGATTTTT
Mmp7	TTCTGCTTTGTGTGTCTGCTG	CCTTCTTTGTTTTAGAGTCATGAGG
Mttp	GGCAGTGCTTTTTCTCTGCT	TGAGAGGCCAGTTGTGTGAC
Muc 2	GCTGACGAGTGGTTGGTGAATG	GATGAGGTGGCAGACAGGAGAC
Muc 3	CGTGGTCAACTGCGAGAATGG	CGGCTCTATCTCTACGCTCTCC
Muc 4	CAGCAGCCAGTGGGGACAG	CTCAGACACGCCAGGGAACTC
c-*myc*	GACAAGAGGCGGACACACAA	GGATGTAGGCGGCTTTT
Neuro-D	GCATGCACGGGCTGAACGC	GGGATGCACCGGGAAGGAAG
Ngn 3	CTTCACAAGAAGTCTGAGAACACCAG	CTGCGCATAGCGGACCACAGCTTC
Ocln	GCTGTGATGTGTGTGAGCTG	GACGGTCTACCTGGAGGAAC
P21	TCCACAGCGATATCCAGACA	GGACATCACCAGGATTGGAC
P27	TCAAACGTGAGAGTGTCTAACGG	AGGGGCTTATGATTCTGAAAGTCG
Pkp2	CGCCTCACCCTGCCACGCTATGCTC	GCGGGCGGTTCTGCTCTGCGTGCTTTGA
Sct	GCTGTGGTCGAACACTCAGA	GAGACAGGGACCCATCCAG
Sox 9	CAGCAAGACTCTGGGCAAG	TCCACGAAGGGTCTCTTCTC
Sst	CCCAGACTCCGTCAGTTTCT	GGGCATCATTCTCTGTCTGG
Tcf 4	CAACGAACACAGCGAATGTT	TTAGGAGCGCTCAGGTCTGT
Tff3	CCTGGTTGCTGGGTCCTCTG	GCCACGGTTGTTACACTGTC
ZO1	AGGACACCAAAGCATGTGAG	GGCATTCCTGCTGGTTACA

[a] The primers were designed in different exons of the corresponding gene, except in those marked with an asterisk, which indicates that the gene has no intron.

RESULTS

Elimination of HNF-4α in the intestinal epithelium of adult mice. To examine the role of HNF-4α in the intestinal epithelium of adult mice, floxed *Hnf-4a* mutant mice (21) containing two *loxP* sites flanking exons 4 and 5 of the *Hnf-4a* gene (*Hnf-4a*$^{loxP/loxP}$ mice) (Fig. 1A, top) were crossed with the villin-Cre-ERT2 line (16) to generate *Hnf-4a*$^{loxP/loxP}$; villin-Cre-ERT2 mice. The expression of HNF-4α was quantified by semiquantitative RT-PCR on mRNA isolated from 2-month-old wild-type mice, *Hnf-4a*$^{loxP/loxP}$ mice, and *Hnf-4a*$^{loxP/loxP}$; villin-Cre-ERT2 mice without CRE recombinase activation. Whatever the genotype, the levels of *Hnf-4a* mRNA were identical and we demonstrated an absence of hypomorphism for *Hnf-4a* gene expression. There was no detectable background recombination in the presence of the villin-Cre-ERT2 transgene and no phenotypic differences between these strains. The different genotypes were equally viable and were obtained at the expected ratios in all crosses (data not shown).

The CRE recombinase activity was induced by daily injection of tamoxifen on 5 consecutive days in 2-month-old mice. The deletion of exons 4 and 5 by the induction of CRE recombinase activity in *Hnf-4a*$^{loxP/loxP}$; villin-Cre-ERT2 mice gener-

ated *Hnf-4a*$^{int\Delta}$ mice (Fig. 1A, top). *Hnf-4a*$^{loxP/loxP}$ mice, i.e., mice lacking the Cre-ERT2 transgene, were used as controls and injected with tamoxifen under the same conditions as the *Hnf-4a*$^{int\Delta}$ mice. Mice were euthanized on day 8 following the first injection, a time interval corresponding at least to one complete intestinal epithelium renewal cycle. The removal of exons 4 and 5 was specific for all segments of the intestine and was not observed in the other organs expressing HNF-4α, i.e., the liver, kidneys, stomach, or pancreas (Fig. 1A, bottom). The inactivation was very efficient, as the drop in *Hnf-4a* mRNA expression reached 90% and 87% in the villus and crypt epithelium of the jejunum, respectively (Fig. 1C). Similar results were obtained in the ileum and colon (data not shown). Accordingly, the level of HNF-4α protein was decreased by 90% in the jejunum epithelium of *Hnf-4a* intestine-null mice (Fig. 1D). As previously shown for wild-type mice (45), HNF-4α was expressed in the nuclei of all epithelial cells along the crypt-to-villus axis in control *Hnf-4a*$^{loxP/loxP}$ mice (Fig. 1E). HNF-4α was not detectable in epithelial cells of *Hnf-4a*$^{int\Delta}$ mice (Fig. 1E) and remained at very low levels up to 30 days after tamoxifen injections (Fig. 2A). Together, these results indicated that injections of tamoxifen resulted in an intestine-specific recombination of the floxed *Hnf-4a* gene in *Hnf-4a*$^{loxP/loxP}$; villin-CreERT2 mice and that the loss of HNF-4α protein was observed in all epithelial cells along the crypt-to-villus axis.

Loss of HNF-4α enhances the proliferation of epithelial cells in crypts. Histological examination of intestinal sections from *Hnf-4a*$^{loxP/loxP}$ and *Hnf-4a*$^{int\Delta}$ mice showed that the general morphology of the intestinal epithelium was conserved in *Hnf-4a*$^{int\Delta}$ mice (Fig. 3A) but that the depths of the crypts were significantly increased in the *Hnf-4a*$^{int\Delta}$ mice (Fig. 3B and C), whereas the sizes of the villi remained similar in the two groups of mice. Within the crypt compartment of *Hnf-4a*$^{int\Delta}$ mice, the size of the cells appeared normal, suggesting that crypt hypertrophy was the consequence of hyperplasia and of aberrant proliferation. To test this hypothesis, *Hnf-4a*$^{int\Delta}$ and *Hnf-4a*$^{loxP/loxP}$ mice were injected with BrdU and euthanized 90 min later. The average number of BrdU-positive cells per crypt was twofold higher in *Hnf-4a*$^{int\Delta}$ mice than in *Hnf-4a*$^{loxP/loxP}$ control mice (Fig. 3D and E). In the colon, where the inactivation of HNF-4α was efficient, the number of proliferative cells was also increased (Fig. 4A and B). The proliferative index (i.e., the ratio of the number of proliferative cells to the total number of cells in the crypt) was higher in *Hnf-4a*$^{int\Delta}$ mice (Fig. 3F), suggesting a loss of intestinal homeostasis. Immunostaining of the Ki67 protein confirmed the increased epithelial proliferation in crypts of *Hnf-4a*$^{int\Delta}$ mice (Fig. 3G). As the length of the villi was not affected, we measured the frequency of apoptosis by immunostaining of the activated caspase 3 in the intestinal epithelium. *Hnf-4a*$^{int\Delta}$ epithelium presented fourfold more activated-caspase 3-positive cells than that of *Hnf-4a*$^{loxP/loxP}$ controls (Fig. 3H and I). This observation could explain the normal length of the villi despite the increased number of proliferative cells.

Interestingly, 30 days after tamoxifen injection, the observed effects on crypt size and proliferation were still significant but less pronounced than those observed 8 days after tamoxifen injection (Fig. 2B, C, and D).

Loss of HNF-4α activates the Wnt/β-catenin signaling pathways. The canonical Wnt pathway was shown to play an important role in maintaining the proliferation capacity of the intestinal epithelium (46). We observed an enhancement of intracellular β-catenin staining in crypts of *Hnf-4a*$^{int\Delta}$ mice compared to that in *Hnf-4a*$^{loxP/loxP}$ control mice (Fig. 5A). We further analyzed the level of nuclear and cytoplasmic β-catenin in crypt cells. The amount of cytoplasmic β-catenin was unchanged (Fig. 5B, top), whereas that of nuclear β-catenin was increased by 50% (Fig. 5B, bottom) in *Hnf-4a*$^{int\Delta}$ mice compared to that in *Hnf-4a*$^{loxP/loxP}$ control mice. The cytoplasmic and nuclear fraction purity was assessed through LDH (cytoplasmic) and Sp1 (nuclear) immunoblot assays. Contamination of the nuclear fraction by cytoplasm was negligible (Fig. 5B). The accumulation of cytoplasmic and nuclear β-catenin is the hallmark of active Wnt signaling; we analyzed the expression of several classical target genes of Wnt pathway activation in crypt-enriched epithelial cells. The expression of Tcf-4, axin 2, c-Myc, and Lgr-5 was significantly increased in *Hnf-4a*$^{int\Delta}$ mice (Fig. 5C). In parallel, the expression of the cell cycle inhibitor p21 was significantly decreased in crypt-enriched (data not

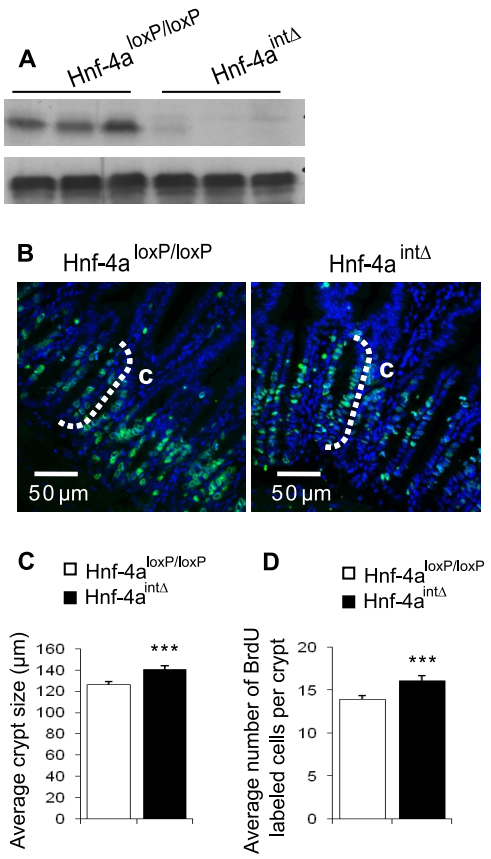

FIG. 2. Cell proliferation in adult intestinal epithelium 30 days after tamoxifen injection. (A) Representative Western blot analysis of HNF-4α protein in epithelial cells from the jejunums of control *Hnf-4a*$^{loxP/loxP}$ and *Hnf-4a*$^{int\Delta}$ mice 30 days following the first injection. (B) BrdU (green) and DAPI (blue) staining in the crypts of jejunums of *Hnf-4a*$^{int\Delta}$ and *Hnf-4a*$^{loxP/loxP}$ mice. The white dashed bracket delimits the crypt compartment. (C) Average lengths of crypts as determined by measuring 40 crypts from *Hnf-4a*$^{int\Delta}$ and *Hnf-4a*$^{loxP/loxP}$ mice ($n = 3$ animals per genotype). (D) Average numbers of BrdU-positive epithelial cells per crypt of *Hnf-4a*$^{int\Delta}$ and *Hnf-4a*$^{loxP/loxP}$ mice ($n = 40$ crypts from three animals per genotype).

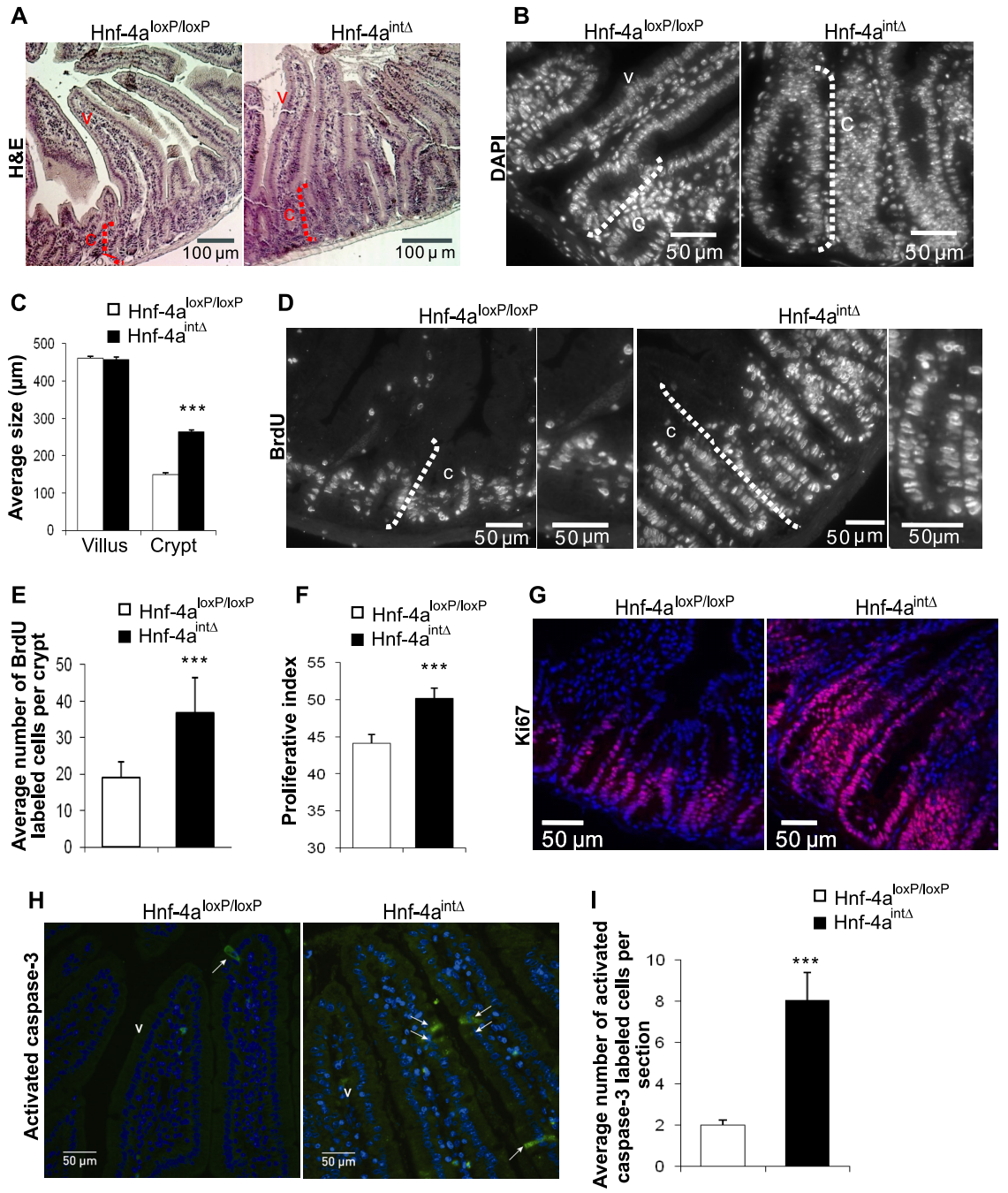

FIG. 3. Increased cell proliferation and death in the absence of HNF-4α in adult intestinal epithelium. (A) Hematoxylin and eosin (H&E) staining of jejunum sections shows the general structure of the crypt-to-villus axis of *Hnf-4a*$^{int\Delta}$ and *Hnf-4a*$^{loxP/loxP}$ mice. Note the crypt size of *Hnf-4a*$^{int\Delta}$ mice compared to that of control *Hnf-4a*$^{loxP/loxP}$ mice. The dashed line indicates the crypt (C), and V marks the villus. (B) DAPI staining to visualize nuclei in the crypts of *Hnf-4a*$^{int\Delta}$ and *Hnf-4a*$^{loxP/loxP}$ mice. The white dashed bracket delimits the crypt compartment. (C) Representation of the average length of crypts and villi as determined by measuring 40 crypts or villi in each *Hnf-4a*$^{int\Delta}$ or *Hnf-4a*$^{loxP/loxP}$ mouse ($n = 9$ animals per genotype). (D) BrdU staining of *Hnf-4a*$^{int\Delta}$ and *Hnf-4a*$^{loxP/loxP}$ jejunum sections showing the progression rate of cells in S phase. The crypt compartment is delimited by the white dashed bracket. (E) Average number of BrdU-positive epithelial cells per crypt of *Hnf-4a*$^{int\Delta}$ and *Hnf-4a*$^{loxP/loxP}$ mice ($n = 70$ crypts from nine animals per genotype). (F) Graphic representation of the proliferative index in crypts of *Hnf-4a*$^{int\Delta}$ and *Hnf-4a*$^{loxP/loxP}$ mice, i.e., percentage of BrdU-positive epithelial cells per number of crypt cells visualized by DAPI staining. (G) Immunostaining of Ki67 in *Hnf-4a*$^{int\Delta}$ and *Hnf-4a*$^{loxP/loxP}$ jejunum sections for the identification of epithelial cells undergoing cell cycle progression. (H) Immunostaining of activated caspase 3 in *Hnf-4a*$^{int\Delta}$ and *Hnf-4a*$^{loxP/loxP}$ jejunum sections for detection of the apoptosis status of epithelial cells. Positive cells are indicated by arrows. (I) Average numbers of activated-caspase 3-positive cells per section of jejunum of *Hnf-4a*$^{int\Delta}$ and *Hnf-4a*$^{loxP/loxP}$ mice. For each graph, an unpaired Student *t* test was used to measure significance. ***, $P < 0.001$. Error bars indicate the standard error of the mean.

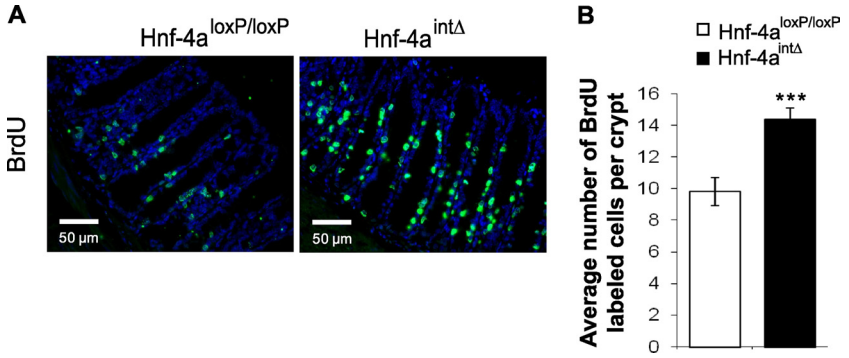

FIG. 4. Proliferation in colon epithelium of mice lacking HNF-4α. (A) Representative BrdU staining in the colons of *Hnf-4a*$^{loxP/loxP}$ and *Hnf-4a*$^{int\Delta}$ mice. (B) Average numbers of BrdU-positive nuclei in epithelia of *Hnf-4a*$^{loxP/loxP}$ and *Hnf-4a*$^{int\Delta}$ mice. For each graph, an unpaired Student *t* test was used to measure significance. ***, $P < 0.001$. Error bars indicate the standard error of the mean.

shown) and villus-enriched epithelial cells from *Hnf-4a*$^{int\Delta}$ mice at both the mRNA (Fig. 5C) and protein (Fig. 5D) levels. No significant change was observed in the expression of p27 (data not shown) or cyclin D1 (Fig. 5C), which are also regulators of the cell cycle.

To further address the relationships between HNF-4α and the Wnt/β-catenin pathway, we transfected the TOP/FOP luciferase reporter vectors, a TCF/β-catenin-directed transcription system (47), together with increasing amount of an HNF-4α-expressing vector, into the HCT116 colon carcinoma cell line, which does not express endogenous HNF-4α (22). HNF-4α strongly (80%) decreased the β-catenin/TCF-dependent luciferase activity in a dose-dependent manner (Fig. 5E). An interaction between HNF-4α and Tcf-4 or β-catenin has been investigated. Through coimmunoprecipitation experiments with HCT116 (Fig. 6A) and Caco-2/TC7 (Fig. 6B) cells, we showed that HNF-4α interacts with Tcf-4 but not with β-catenin. All together, these results, which were obtained in vivo and in vitro, indicated that HNF-4α interfered with the Wnt/β-catenin pathway to control the proliferation of crypt epithelial cells.

Loss of HNF-4α alters the secretory cell lineage in the adult intestinal epithelium. We analyzed the effect of HNF-4α loss on the intestinal epithelial cell lineage. The four differentiated cell types were reported to originate from intestinal stem cells. Activation of the Notch signaling pathway is known to induce *Hes-1* gene expression and commitment of epithelial cells to the absorptive lineage, leading to differentiated enterocytes, through repression of *Math-1*, encoding a transcription factor necessary for cell commitment to the secretory lineage (46). In *Hnf-4a*$^{int\Delta}$ mouse crypts, we observed a 1.8-fold increase in the *Math-1* mRNA level and no significant modification of the *Hes-1* mRNA level (Table 2).

Consistent with this observation, the average number of goblet cells detected by PAS (32) staining was significantly increased (1.3-fold in villi and 1.7-fold in crypts) in *Hnf-4a*$^{int\Delta}$ mice (Fig. 7A and C). The mRNA encoding trefoil factor 3, a marker of differentiated goblet cells, was also increased, as well as that of Muc2, the major gel-forming mucin in goblet cells (Table 2). Goblet cells were mature, as confirmed by PAS staining and electron microscopy (Fig. 7A and B). The loss of HNF-4α affected neither the number of Paneth cells stained with an anti-lysozyme antibody (Fig. 7F) nor the level of *MMP-7* or *Sox-9* mRNA (Table 2). The cryptdin-1 mRNA level was only moderately affected (Table 2). We examined and counted the enteroendocrine cells after immunostaining of chromogranin A (Fig. 7D and E). In *Hnf-4a*$^{int\Delta}$ mice, we observed a 1.4-fold decrease in the enteroendocrine cell number in villi and a 1.4-fold increase in crypts, resulting in an unchanged total (crypts plus villi) enteroendocrine cell number. The expression level of genes encoding the gut hormones glucose-dependent insulinotropic peptide, somatostatin, and glucagon was significantly decreased (Table 2), suggesting that the corresponding endocrine subtypes were reduced. The transcription factors Ngn-3 and NeuroD were reported to be involved in enteroendocrine specification and differentiation (31). The mRNA encoding Ngn-3 was significantly increased in *Hnf-4a*$^{int\Delta}$ mice, whereas that encoding NeuroD remained unchanged (Table 2).

Our previous work (2, 9) and a bioinformatic analysis (49) showed that, in the intestine, HNF-4α influences enterocyte function by regulating genes involved in lipid metabolism. Thus, we analyzed the expression of several genes involved in the function of lipid transfer in enterocytes. In *Hnf-4a*$^{int\Delta}$ mice, there was a significant reduction in the mRNAs coding for microsomal triglyceride transfer protein, apolipoproteins B and AIV, and intestinal fatty acid binding protein (Table 2).

In villi, the expression of some transcription factors such as HNF-1α and Cdx2 was unaffected by the loss of HNF-4α, whereas that of Klf4, a Krüppel-like factor expressed in terminally differentiated mucosecretory cells, was decreased by 30% (Table 2). In crypts, HNF-1β (or Tcf2) expression was significantly increased (Table 2). Notably, the absence of HNF-4α induced a strong expression of HNF-4γ in crypts (Table 2 and Fig. 8A) which was still observed 30 days after tamoxifen injection (Fig. 8B) without modifications of HNF-4γ expression in villi (Table 2).

All together, these results showed that intestinal disruption of the *Hnf-4a* gene perturbed the homeostasis of the intestinal epithelium lineage and the terminal differentiation of enterocytes and of some endocrine subtypes.

HNF-4α controls the epithelial cell architecture. HNF-4α has been shown to be essential for morphological differentiation of hepatocytes by regulating the expression of cell-cell junction-associated proteins (41). We thus investigated the impact of intestinal HNF-4α loss on the cell architecture of adult

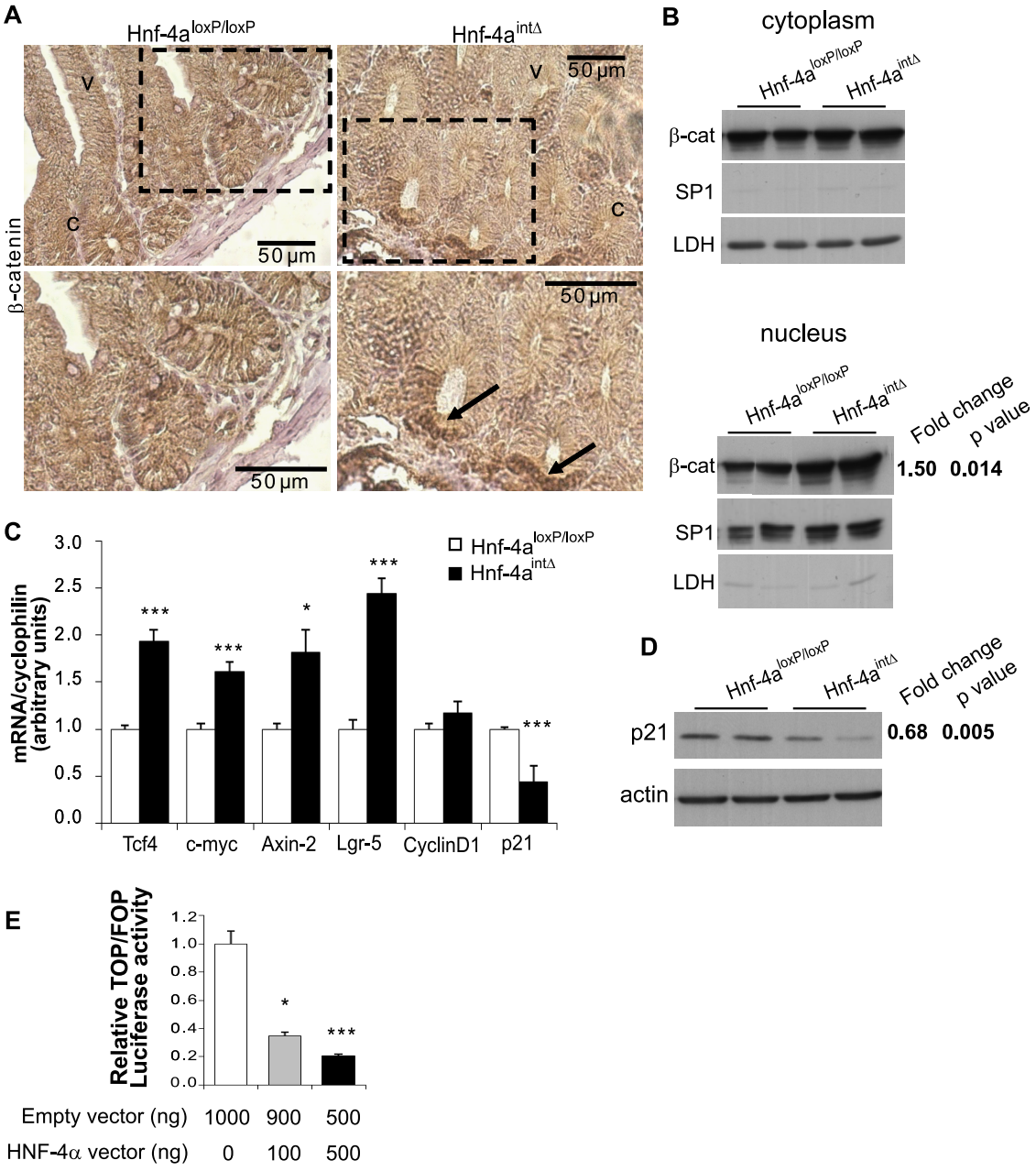

FIG. 5. Loss of HNF-4α enhances Wnt/β-catenin activity in the adult mouse small intestine. (A) Immunohistochemistry of β-catenin in *Hnf-4a*$^{int\Delta}$ and *Hnf-4a*$^{loxP/loxP}$ jejunum sections. Membrane and cytosol immunostained β-catenin is detected by a brown precipitate. Sections were counterstained with hematoxylin (blue). Magnifications of the insets (upper panels), delimited by a black dashed square, are shown (lower panels). Cytosolic accumulation of β-catenin is indicated by arrows. Crypts and villi are indicated by C and V, respectively. (B) The level of nuclear β-catenin (β-cat) is enhanced in the absence of HNF-4α. Immunoblot analysis with an anti-β-catenin antibody in crypts of the jejunum revealed the nuclear and cytoplasmic steady-state levels of β-catenin. Cytoplasmic and nuclear fraction purity was assessed through LDH and SP1 immunoblot assays, respectively. The level of protein expression is expressed relative to the amount present in *Hnf-4a*$^{loxP/loxP}$ mice and is normalized to that of SP1 in the nuclear fraction. Values represent the *n*-fold change in mean expression between *Hnf-4a*$^{int\Delta}$ and *Hnf-4a*$^{loxP/loxP}$ mice ($n = 3$ per genotype). (C) Quantitative RT-PCRs for Wnt target gene expression in adult *Hnf-4a*$^{int\Delta}$ and *Hnf-4a*$^{loxP/loxP}$ jejunum sections. Significant upregulation of Tcf-4, axin 2, c-Myc, and Lgr-5 and significant downregulation of p21 were seen after HNF-4α loss. The mRNA levels are expressed relative to the amount present in *Hnf-4a*$^{loxP/loxP}$ mice and were normalized to the cyclophilin mRNA level. (D) The p21 level is regulated by HNF-4α in the adult jejunum. Immunoblot analysis with an anti-p21 antibody revealed the steady-state levels of p21 and actin (loading control). The value represents the *n*-fold change in the level of p21 expression between *Hnf-4a*$^{int\Delta}$ and *Hnf-4a*$^{loxP/loxP}$ mice and was normalized to that of actin. (E) Overexpression of HNF-4α in HCT116 cells inhibits TOPflash activity. HCT116 cells were transfected with TOPflash, a β-catenin/TCF/LEF-responsive luciferase reporter plasmid containing TCF-4-binding sites, or the corresponding negative control FOPflash, along with HNF-4α and β-galactosidase vectors. Luciferase activity was normalized to the corresponding β-galactosidase activity to obtain the relative TOP/FOP luciferase activity. The graph represents the average luciferase activity ($n = 3$ independent experiments performed in triplicate). For each graph, an unpaired Student *t* test was used to measure significance. ***, **, and *, $P < 0.001$, $P < 0.01$, and $P < 0.05$, respectively. Error bars indicate the standard error of the mean.

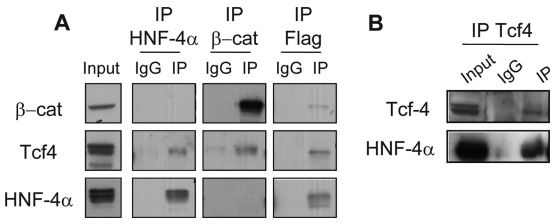

FIG. 6. HNF-4α interacts with Tcf-4 in intestinal epithelial cells. Coimmunoprecipitation analysis of HNF-4α, Tcf-4, and β-catenin (β-cat). (A) Lysates from HCT116 cells transfected with plasmids encoding HNF-4α and Flag-Tcf4 were subjected to immunoprecipitation with anti-HNF-4α, anti-Flag, or anti-β-catenin antibodies as indicated at the top. The input (4% of the total cell extracts) and specific (IP) and nonspecific (IgG) immunoprecipitates were analyzed by Western blotting with the indicated antibodies. (B) Western blot detection of endogenous HNF-4α in Caco-2/TC7 cells after immunoprecipitation with the indicated antibodies.

small intestine epithelium and particularly on the organization of the cell-cell junctions. E-cadherin (adherens junctions) mRNA and protein expression was unchanged in *Hnf-4a*$^{int\Delta}$ mice (Fig. 9A and B), but the protein was not properly located to membranes and was abundantly present in the cytoplasm (Fig. 9C). EBP50 (ERM [ezrin-radixin-meosin] binding protein, also named Na^+/H^+ exchanger regulatory factor 1 or NHERF1) is a scaffolding protein which organizes these ERM proteins at the apical membrane (37), and the gene that encodes it is also a target of HNF-4α (12). Accordingly, the mRNA and protein levels of EBP50 were significantly decreased in *Hnf-4a*$^{int\Delta}$ mice (Fig. 9D and E).

The expression of some genes encoding junctional proteins was further analyzed. Desmocollin 2 and plakophilin 2 (desmosomes) remained unchanged in *Hnf-4a*$^{int\Delta}$ mice, whereas the mRNA encoding Gjb1 (gap junctions) was 1.7-fold increased in mutant mice (Fig. 10A). Important modifications in the expression of tight junction proteins were observed in *Hnf-4a*$^{int\Delta}$ mice, namely, a significant decrease in claudins 4 and 7 and ZO-1 mRNA levels associated with a marked increase in that of claudin 2 (Fig. 10A). These variations correlated with those observed at the protein levels (Fig. 10B and C). Examination of epithelial cell-cell contacts at the ultrastructural level showed that the intercellular space of tight junctions was 1.7-fold wider in *hnf-4*α$^{int\Delta}$ mice than in control mice (Fig. 11A). This structural change might account for the increased paracellular permeability that we quantified both in vivo (Fig. 11B) and ex vivo in Ussing chambers by measuring the mucosal-to-serosal flux of FITC-dextran (Fig. 11C).

DISCUSSION

The results presented here show that the nuclear receptor HNF-4α plays a critical role in the homeostasis of intestinal epithelium, in the epithelial cell architecture, and in the barrier function of the intestine. We report that loss of HNF-4α in the adult small intestine affects the Wnt signaling pathway, leads to enhanced proliferation in crypts, and induces an increased number of mucosecretory cells. In absorptive cells, HNF-4α exerts a major role in the activation of genes involved in lipid transfer by fully differentiated enterocytes (6). Moreover, loss of HNF-4α also disturbs the epithelial cell architecture by modifying the expression of proteins involved in cell-cell adhesion complexes, specifically in the tight junctions, leading to increased in vivo paracellular permeability in *Hnf-4a*$^{int\Delta}$ mice. From these results, we hypothesize that HNF-4α plays dual roles in the adult intestinal epithelium: HNF-4α controls the functional differentiation of epithelial cells and finely modulates the homeostasis of the epithelium.

The importance of HNF-4α as a master regulator of development and differentiation has been established in the liver (15, 29, 41) and in the developing embryonic colon (18). In addition, increasing evidence suggests that HNF-4α plays a role in regulating proliferation. Indeed, HNF-4α was shown to inhibit cell proliferation in vitro (11, 22, 32) and to slow the progression of hepatocellular carcinoma in mice (27). We report here that loss of HNF-4α in the adult intestinal epithelium results in increased cell proliferation in the crypt compartment. This is correlated with downregulation of p21 and overexpression of c-Myc. It was recently reported that HNF-4α increases

TABLE 2. Analysis of gene expression in *Hnf-4a*$^{loxP/loxP}$ and *Hnf-4a*$^{\Delta}$ mouse jejunums

Gene	Compartment[a]	Change in expression[b]
Transcription factors		
Hes-1	C	1.23[c]
Math-1	C	1.86[d]
Ngn-3	V	2.3[e]
NeuroD	V	1.14[c]
Sox-9	C	1.29[c]
Hnf-4g	C	2.46[e]
Hnf-4g	V	1.10[c]
HNF-1a	V	−1.16[c]
HNF-1b	C	1.80[f]
Cdx2	V	−1.09[c]
Klf-4	V	−1.35[f]
Enteroendocrine cell markers		
Gcg	V	−1.56[f]
Gip	V	−1.72[d]
Somatostatin	V	−1.72[d]
Secretin	V	1.09[c]
Paneth cell markers		
MMP-7	C	1.13[c]
Cryptdin-1	C	−1.33[g]
Goblet cell markers		
Muc2	V	1.97[e]
Muc3	V	1.01[c]
Tff-3	V	1.35[g]
Enterocyte cell markers		
Mttp	V	−1.27[e]
ApoB	V	−1.69[d]
ApoA4	V	−1.39[e]
i-FABP	V	−1.45[d]

[a] C, crypt; V, villus epithelium.
[b] Determined by quantitative real-time PCR. All values are the ratio of normalized expression levels of *Hnf-4a*$^{int\Delta}$ to *Hnf-4a*$^{loxP/loxP}$. Negative values indicate reduced gene expression in *Hnf-4a*$^{int\Delta}$ compared to *Hnf-4a*$^{loxP/loxP}$ mouse intestines.
[c] No statistically significant difference.
[d] $P < 0.0001$.
[e] $P < 0.01$.
[f] $P < 0.001$.
[g] $P < 0.05$.

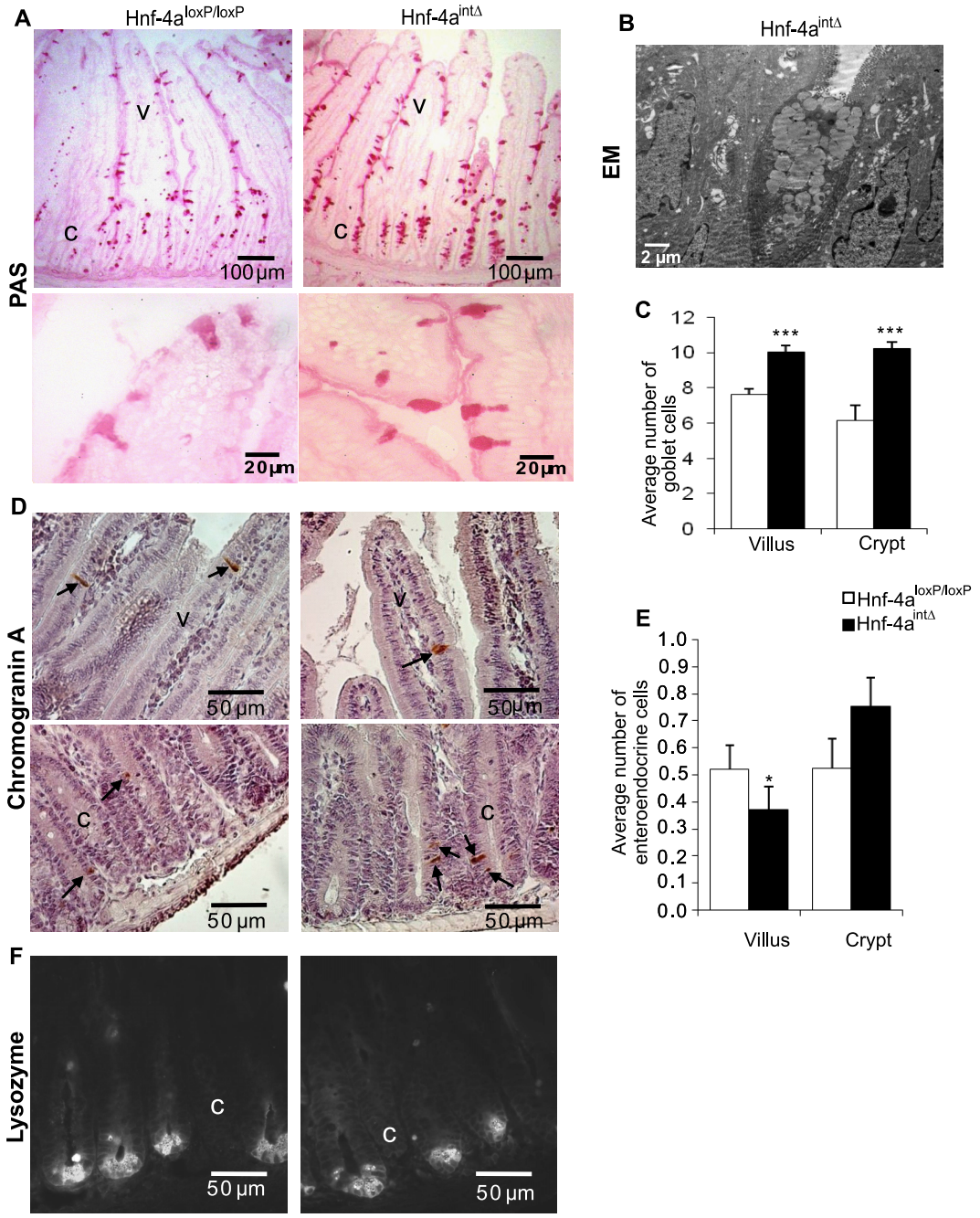

FIG. 7. Altered number of goblet cells in the small intestines of adult *Hnf-4a*$^{int\Delta}$ mice. (A) PAS (32) staining (pink) of goblet cells in adult *Hnf-4a*$^{int\Delta}$ and *Hnf-4a*$^{loxP/loxP}$ jejunums. (B) Electron microscopy showing a mature goblet cell in adult *Hnf-4a*$^{int\Delta}$ jejunum. Optical microscopy shows that the goblet cells are open at the luminal side, and electron microscopy shows that the secretory granules occupy a large portion of the cytoplasm. (C) Average number of PAS-positive jejunum cells of adult *Hnf-4a*$^{int\Delta}$ and *Hnf-4a*$^{loxP/loxP}$ mice per villus or per crypt (n = 8 crypt-to-villus axes and 3 mice per genotype). (D) Chromogranin A immunostaining (brown) and hematoxylin (blue) counterstaining of adult *Hnf-4a*$^{int\Delta}$ and *Hnf-4a*$^{loxP/loxP}$ jejunum sections to visualize enteroendocrine cells. Arrows indicate specific staining of enteroendocrine cells. (E) Average number of chromogranin A-positive cells per villus or per crypt of adult *Hnf-4a*$^{int\Delta}$ and *Hnf-4a*$^{loxP/loxP}$ mouse jejunum (n = 40 crypt-to-villus axes from eight animals per genotype). (F) Immunostaining of lysozyme of adult *Hnf-4a*$^{int\Delta}$ and *Hnf-4a*$^{loxP/loxP}$ mouse jejunum sections to visualize Paneth cells. Crypts and villi are indicated by C and V, respectively. For each graph, an unpaired Student t test was used to measure significance. *** and *, $P < 0.001$ and $P < 0.05$, respectively. Error bars indicate the standard error of the mean.

the expression of the p21 gene by competing with c-Myc for the p21 promoter (11, 22), a mechanism that could account for the downregulation of p21 expression observed in *Hnf-4a*$^{int\Delta}$ mice. The canonical Wnt pathway was shown to play an important role in maintaining the proliferation capacity of the intestinal epithelium (46). Tcf-4, whose intestinal inactivation leads to an absence of proliferating cells, is the most prominent effector of Wnt/β-catenin signaling in the gastrointestinal tract (25, 51).

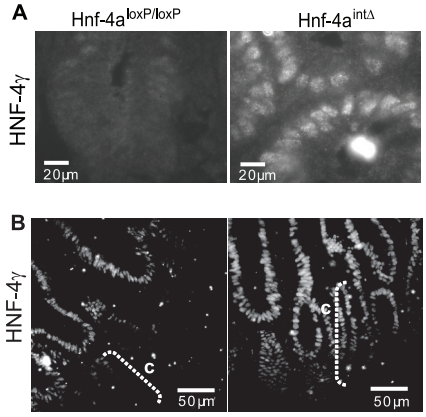

FIG. 8. Expression of HNF-4γ in the absence of HNF-4α. Representative HNF-4γ staining observed in jejunum sections of *Hnf-4a*$^{loxP/loxP}$ and *Hnf-4a*$^{int\Delta}$ mice 8 (A) and 30 (B) days after the first tamoxifen injection.

The expression of Tcf-4 is upregulated in the absence of HNF-4α, concomitantly with that of β-catenin/Tcf-4 target genes, c-Myc, axin 2, Lgr-5, and claudin 2. Furthermore, we demonstrate that HNF-4α is able to decrease Wnt-Tcf4/β-catenin-driven transcription activity. This modulation of the Wnt signaling pathway could be due to an interaction between HNF-4α and Tcf-4 (7) or β-catenin, as shown for other members of the nuclear receptor family (39). Through immunoprecipitation experiments with Caco-2/TC7 and HCT116 cells, we showed that HNF-4α interacts with Tcf-4 but not with β-catenin. One can hypothesized that HNF-4α acts in the crypt to sequester Tcf-4 and thereby represses its transcriptional activity. All together, these observations imply that HNF-4α could regulate the balance between proliferation and differentiation by interfering directly with the Wnt signaling pathway in the intestinal epithelium.

We show here that disrupting *Hnf-4a* gene expression in the intestinal epithelium of adult mice is associated with a marked increase in mucus-secreting cells. In the intestinal epithelium, cells commit either to the absorptive lineage when the Notch signal is activated or to the secretory lineage (enteroendocrine, goblet, and Paneth cells) when the Notch signal is off (46). *Math-1*, which is repressed by the Notch signaling effector Hes-1, is expressed at an early progenitor stage in cells that are committing to the secretory lineage. *Hnf-4a*$^{int\Delta}$ mice show a marked increase in *Math-1* expression, which might explain the higher number of mucus-secreting cells, as well as the upregulation of their differentiation markers trefoil factor 3 and Muc2. Inducible inactivation of the Notch signaling pathway in the adult intestinal epithelium leads to increased expression of *Math-1* with a massive conversion of proliferative crypt cells into goblet cells without impact on the other secreting cells (52). Consistent with these observations, there is no global change in the number of enteroendocrine and Paneth cells in *Hnf-4a*$^{int\Delta}$ mice. However, the number of enteroendocrine cells along the crypt-to-villus axis reveals a paradox: compared with controls, *Hnf-4a*$^{int\Delta}$ mice exhibit more enteroendocrine cells in crypts and fewer in villi, as well as increased expression of *Ngn-3*, which is involved in enteroendocrine specification (31), and decreased expression of some differentiation markers

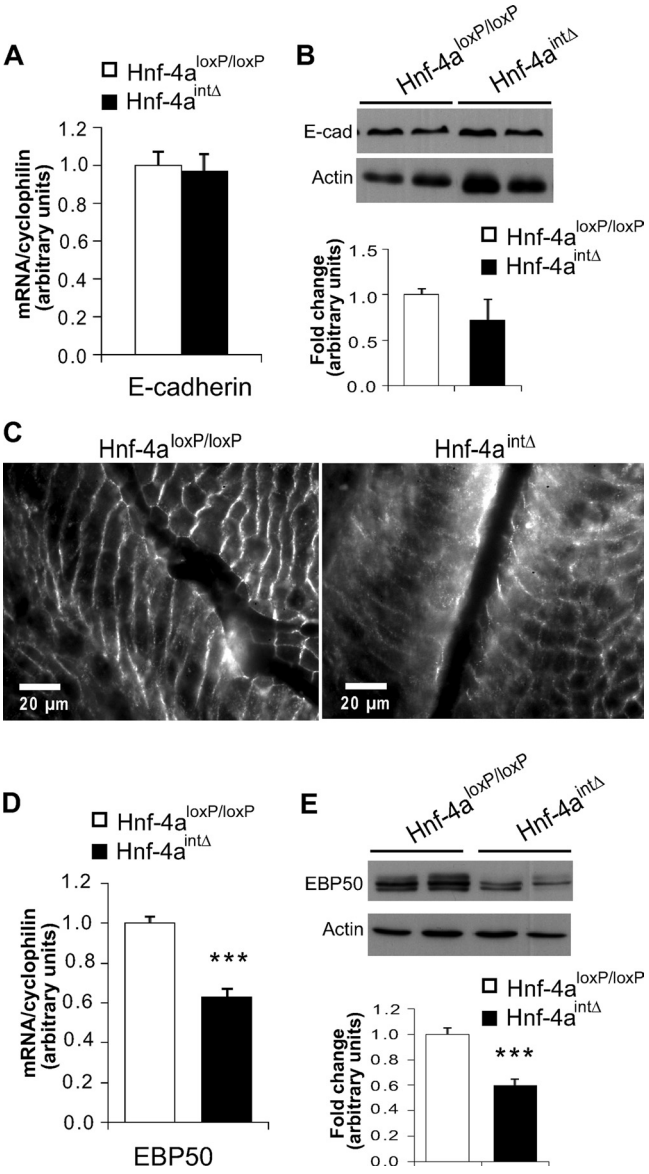

FIG. 9. Expression of E-cadherin and EBP50 in the absence of HNF-4α. (A) The E-cadherin mRNA level from the villus epithelium was analyzed by quantitative RT-PCR in *Hnf-4a*$^{loxP/loxP}$ and *Hnf-4a*$^{int\Delta}$ mice. The mRNA level is expressed relative to the amount present in *Hnf-4a*$^{loxP/loxP}$ mice and is normalized to that of cyclophilin. (B) Representative Western blot analysis of E-cadherin in the villus epithelia of *Hnf-4a*$^{loxP/loxP}$ and *Hnf-4a*$^{int\Delta}$ mice. The histogram represents the quantification of the level of E-cadherin (E-cad) protein ($n = 5$ per genotype). The level of E-cadherin expression is expressed relative to the amount present in *Hnf-4a*$^{loxP/loxP}$ mice and is normalized to that of actin. (C) Immunostaining of E-cadherin in the jejunums of *Hnf-4a*$^{loxP/loxP}$ and *Hnf-4a*$^{int\Delta}$ mice. Note the diffuse staining of E-cadherin in *Hnf-4a*$^{int\Delta}$ mice. (D) The EBP50 mRNA level from the villus epithelium was analyzed by real-time quantitative PCR in *Hnf-4a*$^{loxP/loxP}$ and *Hnf-4a*$^{int\Delta}$ mice. The mRNA level is expressed relative to the amount present in *Hnf-4a*$^{loxP/loxP}$ mice and is normalized to that of cyclophilin. (E) Representative Western blot analysis of EBP50 in the villus epithelia of *Hnf-4a*$^{loxP/loxP}$ and *Hnf-4a*$^{int\Delta}$ mice. The histogram represents the quantification of the level of EBP50 protein ($n = 7$ per genotype). The level of EBP50 expression is expressed relative to the amount present in *Hnf-4a*$^{loxP/loxP}$ mice and is normalized to that of actin expression. For each graph, an unpaired Student *t* test was used to measure significance. ***, $P < 0.001$. Error bars indicate the standard error of the mean.

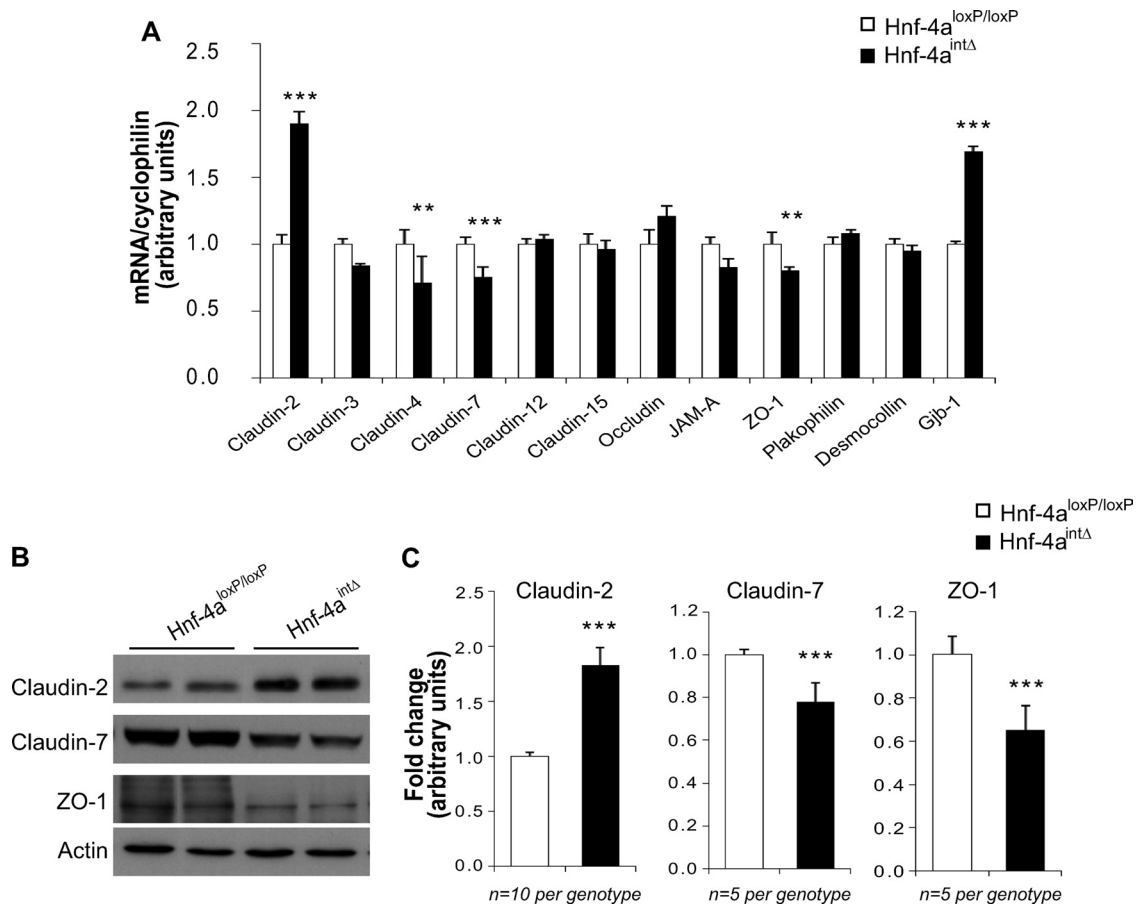

FIG. 10. Expression of tight junction-associated proteins in the absence of HNF-4α. (A) The levels of mRNAs encoding different junction proteins from the villus epithelium were analyzed by quantitative RT-PCR in *Hnf-4a*$^{loxP/loxP}$ and *Hnf-4a*$^{int\Delta}$ mice. mRNA levels are expressed relative to those of *Hnf-4a*$^{loxP/loxP}$ mice and are normalized to the cyclophilin mRNA level. (B) Representative Western blot analysis of claudin 2, claudin 7, and ZO-1 in the jejunums of *Hnf-4a*$^{loxP/loxP}$ and *Hnf-4a*$^{int\Delta}$ mice. (C) Quantification of the expression of tight junction-associated proteins by scanning Western blot analysis. The level of protein expression is expressed relative to the amount present in *Hnf-4a*$^{loxP/loxP}$ mice and is normalized to that of actin. Values represent the *n*-fold changes in mean expression between *Hnf-4a*$^{int\Delta}$ and *Hnf-4a*$^{loxP/loxP}$ mice. For each graph, an unpaired Student *t* test was used to measure significance. *** and **, $P < 0.001$ and $P < 0.01$, respectively. Error bars indicate the standard error of the mean.

such as glucagon, glucose-dependent insulinotropic peptide, and somatostatin. We hypothesize that the higher level of *Ngn-3* mRNA in *Hnf-4a*$^{int\Delta}$ mice drives more cells toward the enteroendocrine lineage but that the absence of HNF-4α prevents their full terminal differentiation. Commitment to the absorptive lineage is driven by the Notch signal and the transcriptional factor Hes-1. In *Hnf-4a*$^{int\Delta}$ mice, the expression of *Hes-1* and the number of enterocytes, estimated by the size of villi, are unchanged. Thus, the main role of HNF-4α in the absorptive cells is to control genes specifically expressed in fully differentiated enterocytes, notably, those involved in the transfer of dietary lipids.

It is noteworthy that *Hnf-4g*, the paralog of *Hnf-4a*, is expressed in intestinal villi (45) but not in the liver (50). Our results suggest that HNF-4γ, whose expression is similar in the villus compartment and induced in the crypt compartment of *Hnf-4a*$^{int\Delta}$ mice, may act to partly compensate for the lack of HNF-4α. This hypothesis is supported by the observation that HNF-4γ is still present in crypts at 30 days after tamoxifen injections. At this time, the size of crypts and the proliferation status are closer to those of control mice. A recent paper from Babeu et al. (3) reported results obtained with mice where the same *Hnf-4a*$^{loxP/loxP}$ gene was inactivated in the intestine but by using a constitutively active Cre recombinase driven by a 12.5-kbp villin promoter which is active at embryonic days 12.5 to 13.5 (34). The animals were viable and did not present any overt phenotype or intestinal dysfunction. The results we obtained with adults 30 days after tamoxifen injection are similar to those of Babeu et al. (3), i.e., a subtle and statistically significant increase in crypt cell proliferation and of the number of goblet cells. Our observations support the hypothesis of functional compensation by HNF-4γ. It may be hypothesized that in the study of Babeu et al., the absence of an overt phenotype could be due to the presence of HNF-4γ, even if a slight decrease in the expression of *Hnf-4g* was observed in the whole intestinal epithelium of their mice. We have previously reported that, in vitro, the two isoforms have similar properties, i.e., affinity for their binding site and transactivation of a reporter gene (2). However, mice lacking expression of HNF-4γ are viable and have no evident phenotype, indicating

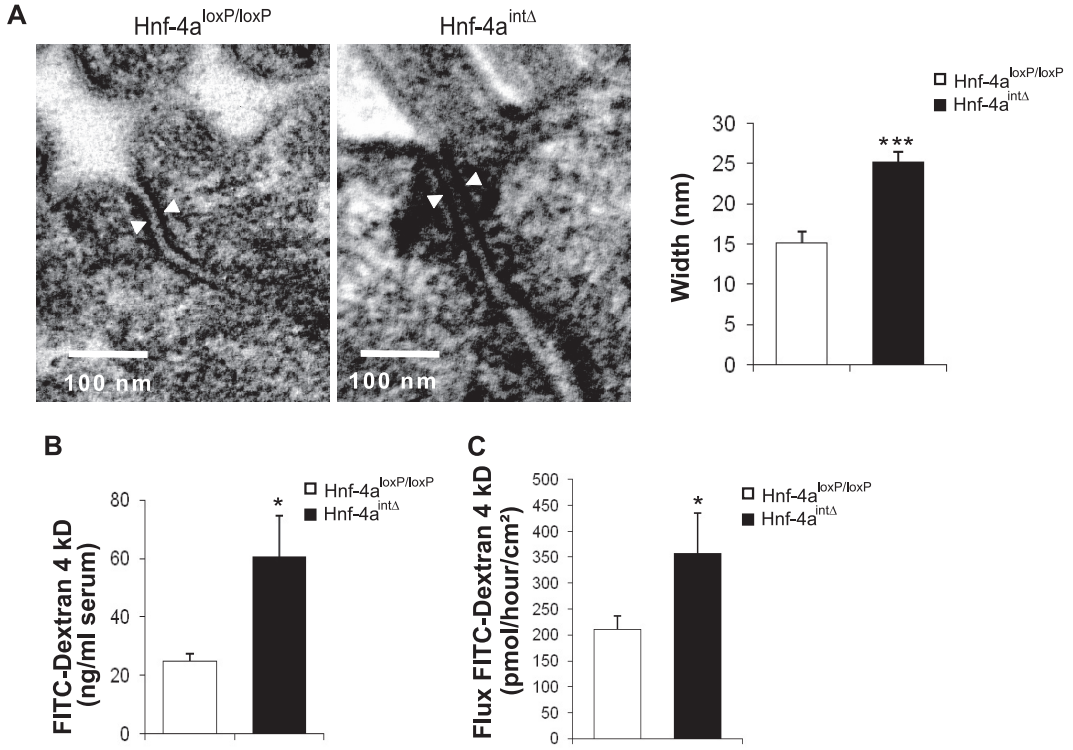

FIG. 11. Distension of tight junctions and increased paracellular permeability in the absence of HNF-4α. (A) Electron microscopic images showing the intercellular space in tight junctions of *Hnf-4a*$^{loxP/loxP}$ and *Hnf-4a*$^{int\Delta}$ mice. The histogram represents the average width of tight junctions, measured between the two external membranes, as indicated by arrowheads (8 to 12 junctions and three animals per genotype). (B) In vivo paracellular permeability analysis done by measuring the FITC-dextran in serum samples from *Hnf-4a*$^{loxP/loxP}$ and *Hnf-4a*$^{int\Delta}$ mice ($n = 9$ animals per genotype). (C) Paracellular permeability analysis done by measuring FITC-dextran flux in Ussing chambers with *Hnf-4a*$^{loxP/loxP}$ and *Hnf-4a*$^{int\Delta}$ mouse intestine sections ($n = 12$ animals per genotype.). For each graph, an unpaired Student *t* test was used to measure significance. *** and *, $P < 0.001$ and $P < 0.05$, respectively. Error bars indicate the standard error of the mean.

that the two proteins are not fully redundant. Deciphering the different roles of the two isoforms is still a challenging task.

HNF-4α plays an essential role in the architecture of epithelial cells (5, 10, 12, 41, 48). In the adult intestinal epithelium, loss of HNF-4α induces a distension of tight junctions that is associated with changes in the expression of tight junction proteins such as claudins 2, 4, and 7 and ZO-1. These modifications could be due to the increased expression of Tcf-4, which is a negative regulator of claudin 7 expression and a positive regulator of claudin 2 expression (13). Claudins are responsible for the gate function of tight junctions, which control paracellular permeability. Increased claudin 2 expression was reported to be responsible for increased epithelial permeability (54). Accordingly, we observed an increased paracellular permeability of *Hnf-4a*$^{int\Delta}$ mouse intestine in vivo and in vitro. Interestingly, HNF-4α has recently been shown to have a role in protection against inflammatory bowel diseases, a pathology where the epithelial barrier is impaired (1). Furthermore, loss of tight junction structure and function is frequently observed in epithelium-derived cancers and overexpression of claudin 2 can stimulate the invasion and migration activities of cancer cells (36). Loss of HNF-4α in intestinal epithelium also induces a drastic decrease in EBP50 expression. ERM proteins regulate the organization and function of specific cortical structures in polarized epithelial cells, and EBP50 organizes these ERM proteins at the apical membrane (37). The observed downregulation of EBP50 expression in *Hnf-4a*$^{int\Delta}$ mice could explain the concomitant E-cadherin membrane delocalization. Indeed, low expression of EBP50 decreased the interaction between β-catenin and E-cadherin, leading to disorganization of adherens junctions and increased cell proliferation and motility (26).

Our work in vivo demonstrates for the first time that HNF-4α is a transcription factor at the crossroads between intestinal epithelium homeostasis and epithelial cell architecture in the adult mouse intestine by controlling cell proliferation in crypts and functional differentiation in villi. Indeed, HNF-4α interferes with the Wnt/β-catenin signaling pathway and its loss destabilizes adherens and tight junctions. It is currently admitted that the deregulation of the Wnt/β-catenin signaling pathway is an early event in the colorectal cancer progression cascade and that the destabilization of cell-cell contacts takes part in the epithelial-to-mesenchymal transition, a crucial process in tumor progression. Since HNF-4α regulates the balance between proliferation and differentiation, we hypothesize that it might act as a tumor suppressor.

ACKNOWLEDGMENTS

We thank N. Comuce, C. Lasne, and V. Chauffeton for animal care. Electron microscopy analysis was performed by using facilities of the Centre de Recherche des Cordeliers, UMRS 872. We thank M. Pontoglio for helpful scientific discussions and access to unpublished re-

sults, J. M. Lacorte and V. Carrière for their help during genotyping and RT-PCR experiments, respectively, and M. Rousset for critical reading of the manuscript.

This work was supported by INSERM, France, and Pierre & Marie Curie University, Paris, France. A.-L. Cattin is the recipient of a doctoral fellowship from the Ministère de l'Enseignement Supérieur et de la Recherche.

REFERENCES

1. **Ahn, S. H., Y. M. Shah, J. Inoue, K. Morimura, I. Kim, S. Yim, G. Lambert, R. Kurotani, K. Nagashima, F. J. Gonzalez, and Y. Inoue.** 2008. Hepatocyte nuclear factor 4α in the intestinal epithelial cells protects against inflammatory bowel disease. Inflamm. Bowel Dis. **14:**908–920.
2. **Archer, A., D. Sauvaget, V. Chauffeton, P. E. Bouchet, J. Chambaz, M. Pincon-Raymond, P. Cardot, A. Ribeiro, and M. Lacasa.** 2005. Intestinal apolipoprotein A-IV gene transcription is controlled by two hormone-responsive elements: a role for hepatic nuclear factor-4 isoforms. Mol. Endocrinol. **19:**2320–2334.
3. **Babeu, J. P., M. Darsigny, C. R. Lussier, and F. Boudreau.** 2009. Hepatocyte nuclear factor 4α contributes to an intestinal epithelial phenotype in vitro and plays a partial role in mouse intestinal epithelium differentiation. Am. J. Physiol. Gastrointest. Liver Physiol. **297:**G124–G134.
4. **Barreau, F., U. Meinzer, F. Chareyre, D. Berrebi, M. Niwa-Kawakita, M. Dussaillant, B. Foligne, V. Ollendorff, M. Heyman, S. Bonacorsi, T. Lesuffleur, G. Sterkers, M. Giovannini, and J. P. Hugot.** 2007. CARD15/NOD2 is required for Peyer's patches homeostasis in mice. PLoS ONE **2:**e523.
5. **Battle, M. A., G. Konopka, F. Parviz, A. L. Gaggl, C. Yang, F. M. Sladek, and S. A. Duncan.** 2006. Hepatocyte nuclear factor 4α orchestrates expression of cell adhesion proteins during the epithelial transformation of the developing liver. Proc. Natl. Acad. Sci. USA **103:**8419–8424.
6. **Béaslas, O., F. Torreilles, P. Casellas, D. Simon, G. Fabre, M. Lacasa, F. Delers, J. Chambaz, M. Rousset, and V. Carrière.** 2008. Transcriptome response of enterocytes to dietary lipids: impact on cell architecture, signaling, and metabolism genes. Am. J. Physiol. Gastrointest. Liver Physiol. **295:**G942–G952.
7. **Benahmed, F., I. Gross, S. J. Gaunt, F. Beck, F. Jehan, C. Domon-Dell, E. Martin, M. Kedinger, J. N. Freund, and I. Duluc.** 2008. Multiple regulatory regions control the complex expression pattern of the mouse Cdx2 homeobox gene. Gastroenterology **135:**1238–1247.e1-3.
8. **Benoit, G., A. Cooney, V. Giguere, H. Ingraham, M. Lazar, G. Muscat, T. Perlmann, J. P. Renaud, J. Schwabe, F. Sladek, M. J. Tsai, and V. Laudet.** 2006. International Union of Pharmacology. LXVI. Orphan nuclear receptors. Pharmacol. Rev. **58:**798–836.
9. **Carrière, V., R. Vidal, C. Lazou, M. Lacasa, F. Delers, A. Ribeiro, M. Rousset, J. Chambaz, and J. M. Lacorte.** 2005. HNF-4-dependent induction of apolipoprotein A-IV gene transcription by an apical supply of lipid micelles in intestinal cells. J. Biol. Chem. **280:**5406–5413.
10. **Chiba, H., T. Gotoh, T. Kojima, S. Satohisa, K. Kikuchi, M. Osanai, and N. Sawada.** 2003. Hepatocyte nuclear factor (HNF)-4α triggers formation of functional tight junctions and establishment of polarized epithelial morphology in F9 embryonal carcinoma cells. Exp. Cell Res. **286:**288–297.
11. **Chiba, H., T. Itoh, S. Satohisa, N. Sakai, H. Noguchi, M. Osanai, T. Kojima, and N. Sawada.** 2005. Activation of p21CIP1/WAF1 gene expression and inhibition of cell proliferation by overexpression of hepatocyte nuclear factor-4α. Exp. Cell Res. **302:**11–21.
12. **Chiba, H., N. Sakai, M. Murata, M. Osanai, T. Ninomiya, T. Kojima, and N. Sawada.** 2006. The nuclear receptor hepatocyte nuclear factor 4α acts as a morphogen to induce the formation of microvilli. J. Cell Biol. **175:**971–980.
13. **Darido, C., M. Buchert, J. Pannequin, P. Bastide, H. Zalzali, T. Mantamadiotis, J. F. Bourgaux, V. Garambois, P. Jay, P. Blache, D. Joubert, and F. Hollande.** 2008. Defective claudin-7 regulation by Tcf-4 and Sox-9 disrupts the polarity and increases the tumorigenicity of colorectal cancer cells. Cancer Res. **68:**4258–4268.
14. **Drewes, T., S. Senkel, B. Holewa, and G. U. Ryffel.** 1996. Human hepatocyte nuclear factor 4 isoforms are encoded by distinct and differentially expressed genes. Mol. Cell. Biol. **16:**925–931.
15. **Duncan, S. A., A. Nagy, and W. Chan.** 1997. Murine gastrulation requires HNF-4 regulated gene expression in the visceral endoderm: tetraploid rescue of Hnf-4$^{-/-}$ embryos. Development **124:**279–287.
16. **el Marjou, F., K. P. Janssen, B. H. Chang, M. Li, V. Hindie, L. Chan, D. Louvard, P. Chambon, D. Metzger, and S. Robine.** 2004. Tissue-specific and inducible Cre-mediated recombination in the gut epithelium. Genesis **39:**186–193.
17. **Fouquet, S., V. H. Lugo-Martínez, A. M. Faussat, F. Renaud, P. Cardot, J. Chambaz, M. Pincon-Raymond, and S. Thenet.** 2004. Early loss of E-cadherin from cell-cell contacts is involved in the onset of anoikis in enterocytes. J. Biol. Chem. **279:**43061–43069.
18. **Garrison, W. D., M. A. Battle, C. Yang, K. H. Kaestner, F. M. Sladek, and S. A. Duncan.** 2006. Hepatocyte nuclear factor 4α is essential for embryonic development of the mouse colon. Gastroenterology **130:**1207–1220.
19. **Gerdin, A. K., V. V. Surve, M. Jonsson, M. Bjursell, M. Bjorkman, A. Edenro, M. Schuelke, A. Saad, S. Bjurstrom, E. J. Lundgren, M. Snaith, R. Fransson-Steen, J. Tornell, A.-L. Berg, and Y. M. Bohlooly.** 2006. Phenotypic screening of hepatocyte nuclear factor (HNF) 4-γ receptor knockout mice. Biochem. Biophys. Res. Commun. **349:**825–832.
20. **Gupta, R. K., and K. H. Kaestner.** 2004. HNF-4α: from MODY to late-onset type 2 diabetes. Trends Mol. Med. **10:**521–524.
21. **Hayhurst, G. P., Y. H. Lee, G. Lambert, J. M. Ward, and F. J. Gonzalez.** 2001. Hepatocyte nuclear factor 4α (nuclear receptor 2A1) is essential for maintenance of hepatic gene expression and lipid homeostasis. Mol. Cell. Biol. **21:**1393–1403.
22. **Hwang-Verslues, W. W., and F. M. Sladek.** 2008. Nuclear receptor HNF4α1 competes with oncoprotein c-Myc for control of the p21/WAF1 promoter. Mol. Endocrinol. **22:**78–90.
23. **Idogawa, M., M. Masutani, M. Shitashige, K. Honda, T. Tokino, Y. Shinomura, K. Imai, S. Hirohashi, and T. Yamada.** 2007. Ku70 and poly(ADP-ribose) polymerase-1 competitively regulate β-catenin and T-cell factor-4-mediated gene transactivation: possible linkage of DNA damage recognition and Wnt signaling. Cancer Res. **67:**911–918.
24. **Idogawa, M., T. Yamada, K. Honda, S. Sato, K. Imai, and S. Hirohashi.** 2005. Poly(ADP-ribose) polymerase-1 is a component of the oncogenic T-cell factor-4/β-catenin complex. Gastroenterology **128:**1919–1936.
25. **Korinek, V., N. Barker, P. Moerer, E. van Donselaar, G. Huls, P. J. Peters, and H. Clevers.** 1998. Depletion of epithelial stem-cell compartments in the small intestine of mice lacking Tcf-4. Nat. Genet. **19:**379–383.
26. **Kreimann, E. L., F. C. Morales, J. de Orbeta-Cruz, Y. Takahashi, H. Adams, T. J. Liu, P. D. McCrea, and M. M. Georgescu.** 2007. Cortical stabilization of β-catenin contributes to NHERF1/EBP50 tumor suppressor function. Oncogene **26:**5290–5299.
27. **Lazarevich, N. L., O. A. Cheremnova, E. V. Varga, D. A. Ovchinnikov, E. I. Kudrjavtseva, O. V. Morozova, D. I. Fleishman, N. V. Engelhardt, and S. A. Duncan.** 2004. Progression of HCC in mice is associated with a downregulation in the expression of hepatocyte nuclear factors. Hepatology **39:**1038–1047.
28. **Le Beyec, J., V. Chauffeton, H. Y. Kan, P. L. Janvier, C. Cywiner-Golenzer, F. P. Chatelet, A. D. Kalopissis, V. Zannis, J. Chambaz, M. Pincon-Raymond, and P. Cardot.** 1999. The −700/−310 fragment of the apolipoprotein A-IV gene combined with the −890/−500 apolipoprotein C-III enhancer is sufficient to direct a pattern of gene expression similar to that for the endogenous apolipoprotein A-IV gene. J. Biol. Chem. **274:**4954–4961.
29. **Li, J., G. Ning, and S. A. Duncan.** 2000. Mammalian hepatocyte differentiation requires the transcription factor HNF-4α. Genes Dev. **14:**464–474.
30. **Li, X., B. B. Madison, W. Zacharias, A. Kolterud, D. States, and D. L. Gumucio.** 2007. Deconvoluting the intestine: molecular evidence for a major role of the mesenchyme in the modulation of signaling cross talk. Physiol. Genomics **29:**290–301.
31. **López-Díaz, L., R. N. Jain, T. M. Keeley, K. L. VanDussen, C. S. Brunkan, D. L. Gumucio, and L. C. Samuelson.** 2007. Intestinal neurogenin 3 directs differentiation of a bipotential secretory progenitor to endocrine cell rather than goblet cell fate. Dev. Biol. **309:**298–305.
32. **Lucas, B., K. Grigo, S. Erdmann, J. Lausen, L. Klein-Hitpass, and G. U. Ryffel.** 2005. HNF4α reduces proliferation of kidney cells and affects genes deregulated in renal cell carcinoma. Oncogene **24:**6418–6431.
33. **Lugo-Martínez, V. H., C. S. Petit, S. Fouquet, J. Le Beyec, J. Chambaz, M. Pincon-Raymond, P. Cardot, and S. Thenet.** 2009. Epidermal growth factor receptor is involved in enterocyte anoikis through the dismantling of E-cadherin-mediated junctions. Am. J. Physiol. Gastrointest. Liver Physiol. **296:**G235–G244.
34. **Madison, B. B., L. Dunbar, X. T. Qiao, K. Braunstein, E. Braunstein, and D. L. Gumucio.** 2002. *cis* elements of the villin gene control expression in restricted domains of the vertical (crypt) and horizontal (duodenum, cecum) axes of the intestine. J. Biol. Chem. **277:**33275–33283.
35. **Mariadason, J. M., C. Nicholas, K. E. L'Italien, M. Zhuang, H. J. Smartt, B. G. Heerdt, W. Yang, G. A. Corner, A. J. Wilson, L. Klampfer, D. Arango, and L. H. Augenlicht.** 2005. Gene expression profiling of intestinal epithelial cell maturation along the crypt-villus axis. Gastroenterology **128:**1081–1088.
36. **Mima, S., M. Takehara, H. Takada, T. Nishimura, T. Hoshino, and T. Mizushima.** 2008. NSAIDs suppress the expression of claudin-2 to promote invasion activity of cancer cells. Carcinogenesis **29:**1994–2000.
37. **Morales, F. C., Y. Takahashi, E. L. Kreimann, and M. M. Georgescu.** 2004. Ezrin-radixin-moesin (ERM)-binding phosphoprotein 50 organizes ERM proteins at the apical membrane of polarized epithelia. Proc. Natl. Acad. Sci. USA **101:**17705–17710.
38. **Morel, E., S. Fouquet, C. Strup-Perrot, C. P. Thievend, C. Petit, D. Loew, A. M. Faussat, L. Yvernault, M. Pincon-Raymond, J. Chambaz, M. Rousset, S. Thenet, and C. Clair.** 2008. The cellular prion protein PrP is involved in the proliferation of epithelial cells and in the distribution of junction-associated proteins. PLoS ONE **3:**e3000.
39. **Mulholland, D. J., S. Dedhar, G. A. Coetzee, and C. C. Nelson.** 2005. Interaction of nuclear receptors with the Wnt/β-catenin/Tcf signaling axis: Wnt you like to know? Endocrinol. Rev. **26:**898–915.
40. **Napolitano, L. M., M. J. Koruda, A. A. Meyer, and C. C. Baker.** 1996. The

impact of femur fracture with associated soft tissue injury on immune function and intestinal permeability. Shock **5:**202–207.

41. **Parviz, F., C. Matullo, W. D. Garrison, L. Savatski, J. W. Adamson, G. Ning, K. H. Kaestner, J. M. Rossi, K. S. Zaret, and S. A. Duncan.** 2003. Hepatocyte nuclear factor 4α controls the development of a hepatic epithelium and liver morphogenesis. Nat. Genet. **34:**292–296.
42. **Plengvidhya, N., A. Antonellis, L. T. Wogan, A. Poleev, M. Borgschulze, J. H. Warram, G. U. Ryffel, A. S. Krolewski, and A. Doria.** 1999. Hepatocyte nuclear factor-4γ: cDNA sequence, gene organization, and mutation screening in early-onset autosomal-dominant type 2 diabetes. Diabetes **48:**2099–2102.
43. **Ribeiro, A., A. Archer, J. Le Beyec, A.-L. Cattin, S. Saint-Just, M. Pinçon-Raymond, J. Chambaz, M. Lacasa, and P. Cardot.** 2007. Hepatic nuclear factor-4, a key transcription factor at the crossroads between architecture and function of epithelia. Recent Patents Endocr. Metab. Immune Drug Discov. **1:**176–181.
44. **Sansom, O. J., V. S. Meniel, V. Muncan, T. J. Phesse, J. A. Wilkins, K. R. Reed, J. K. Vass, D. Athineos, H. Clevers, and A. R. Clarke.** 2007. Myc deletion rescues Apc deficiency in the small intestine. Nature **446:**676–679.
45. **Sauvaget, D., V. Chauffeton, D. Citadelle, F. P. Chatelet, C. Cywiner-Golenzer, J. Chambaz, M. Pincon-Raymond, P. Cardot, J. Le Beyec, and A. Ribeiro.** 2002. Restriction of apolipoprotein A-IV gene expression to the intestine villus depends on a hormone-responsive element and parallels differential expression of the hepatic nuclear factor 4α and γ isoforms. J. Biol. Chem. **277:**34540–34548.
46. **Scoville, D. H., T. Sato, X. C. He, and L. Li.** 2008. Current view: intestinal stem cells and signaling. Gastroenterology **134:**849–864.
47. **Shitashige, M., R. Satow, K. Honda, M. Ono, S. Hirohashi, and T. Yamada.** 2008. Regulation of Wnt signaling by the nuclear pore complex. Gastroenterology **134:**1961–1971.e1-4.
48. **Späth, G. F., and M. C. Weiss.** 1998. Hepatocyte nuclear factor 4 provokes expression of epithelial marker genes, acting as a morphogen in dedifferentiated hepatoma cells. J. Cell Biol. **140:**935–946.
49. **Stegmann, A., M. Hansen, Y. Wang, J. B. Larsen, L. R. Lund, L. Ritie, J. K. Nicholson, B. Quistorff, P. Simon-Assmann, J. T. Troelsen, and J. Olsen.** 2006. Metabolome, transcriptome, and bioinformatic *cis*-element analyses point to HNF-4 as a central regulator of gene expression during enterocyte differentiation. Physiol. Genomics **27:**141–155.
50. **Taraviras, S., T. Mantamadiotis, T. Dong-Si, A. Mincheva, P. Lichter, T. Drewes, G. U. Ryffel, A. P. Monaghan, and G. Schutz.** 2000. Primary structure, chromosomal mapping, expression and transcriptional activity of murine hepatocyte nuclear factor 4γ. Biochim. Biophys. Acta **1490:**21–32.
51. **van de Wetering, M., E. Sancho, C. Verweij, W. de Lau, I. Oving, A. Hurlstone, K. van der Horn, E. Batlle, D. Coudreuse, A. P. Haramis, M. Tjon-Pon-Fong, P. Moerer, M. van den Born, G. Soete, S. Pals, M. Eilers, R. Medema, and H. Clevers.** 2002. The β-catenin/TCF-4 complex imposes a crypt progenitor phenotype on colorectal cancer cells. Cell **111:**241–250.
52. **van Es, J. H., M. E. van Gijn, O. Riccio, M. van den Born, M. Vooijs, H. Begthel, M. Cozijnsen, S. Robine, D. J. Winton, F. Radtke, and H. Clevers.** 2005. Notch/γ-secretase inhibition turns proliferative cells in intestinal crypts and adenomas into goblet cells. Nature **435:**959–963.
53. **Xie, Y., E. P. Newberry, S. G. Young, S. Robine, R. L. Hamilton, J. S. Wong, J. Luo, S. Kennedy, and N. O. Davidson.** 2006. Compensatory increase in hepatic lipogenesis in mice with conditional intestine-specific Mttp deficiency. J. Biol. Chem. **281:**4075–4086.
54. **Zeissig, S., N. Burgel, D. Gunzel, J. Richter, J. Mankertz, U. Wahnschaffe, A. J. Kroesen, M. Zeitz, M. Fromm, and J. D. Schulzke.** 2007. Changes in expression and distribution of claudin 2, 5 and 8 lead to discontinuous tight junctions and barrier dysfunction in active Crohn's disease. Gut **56:**61–72.